Published in final edited form as:
Cell Rep. 2021 November 09; 37(6): 109961. doi:10.1016/j.celrep.2021.109961.

Temporal dynamics of persistent germinal centers and memory B cell differentiation following respiratory virus infection

William T. Yewdell[1,*], **Ryan M. Smolkin**[#2], **Kalina T. Belcheva**[#3], **Alejandra Mendoza**[1], **Anthony J. Michaels**[4], **Montserrat Cols**[1], **Davide Angeletti**[5], **Jonathan W. Yewdell**[6], **Jayanta Chaudhuri**[1,2,4,8,*]

[1]Immunology Program, Memorial Sloan Kettering Cancer Center, New York, NY 10065, USA

[2]Gerstner Sloan Kettering Graduate School of Biomedical Sciences, New York, NY 10065, USA

[3]Biochemistry, Cellular, and Molecular Biology Allied Program, Weill Cornell Graduate School of Medical Sciences, New York, NY 10065, USA

[4]Immunology and Microbial Pathogenesis Program, Weill Cornell Graduate School of Medical Sciences, New York, NY 10065, USA

[5]Department of Microbiology and Immunology, Institute of Biomedicine, University of Gothenburg, 41390 Gothenburg, Sweden

[6]Laboratory of Viral Diseases, National Institutes of Allergy and Infectious Diseases, National Institutes of Health, Bethesda, MD 20892, USA

[#] These authors contributed equally to this work.

Summary

Following infection or immunization, memory B cells (MBCs) and long-lived plasma cells provide humoral immunity that can last for decades. Most principles of MBC biology have been determined with hapten-protein carrier models or fluorescent protein immunizations. Here, we examine the temporal dynamics of the germinal center (GC) B cell and MBC response following mouse influenza A virus infection. We find that antiviral B cell responses within the lung-draining mediastinal lymph node (mLN) and the spleen are distinct in regard to duration, enrichment for antigen-binding cells, and class switching dynamics. While splenic GCs dissolve after 6 weeks post-infection, mLN hemagglutinin-specific (HA^+) GCs can persist for 22 weeks. Persistent GCs continuously differentiate MBCs, with “peak” and “late” GCs contributing equal numbers of HA^+ MBCs to the long-lived compartment. Our findings highlight critical aspects of persistent GC

[*]**Correspondence**: yewdellw@mskcc.org (W.T.Y.), chaudhuj@mskcc.org (J.C.).
[8]Lead contact

Author Contributions

Conceptualization, W.T.Y and J.C.; methodology, W.T.Y., R.M.S., K.T.B.,D.A., and J.C.; validation, W.T.Y., R.S., and K.T.B.; formal analysis, W.T.Y., R.S., and K.T.B.; investigation, W.T.Y., R.S., K.T.B., A.M., and M.C.; writing - original draft, W.T.Y.; writing - review & editing, W.T.Y., R.S., K.T.B., A.M., A.J.M., D.A., J.W.Y., and J.C.; visualization, W.T.Y., R.S., and K.T.B.; data curation, R.S. and K.T.B.; resources, A.M., A.J.M., D.A., and J.W.Y.; supervision, W.T.Y. and J.C.; project administration, W.T.Y. and J.C.; funding acquisition, W.T.Y. and J.C.

Declaration of Interests

The authors declare no competing interests.

Europe PMC Funders Author Manuscripts

responses and MBC differentiation following respiratory virus infection with direct implications for developing effective vaccination strategies.

Abstract

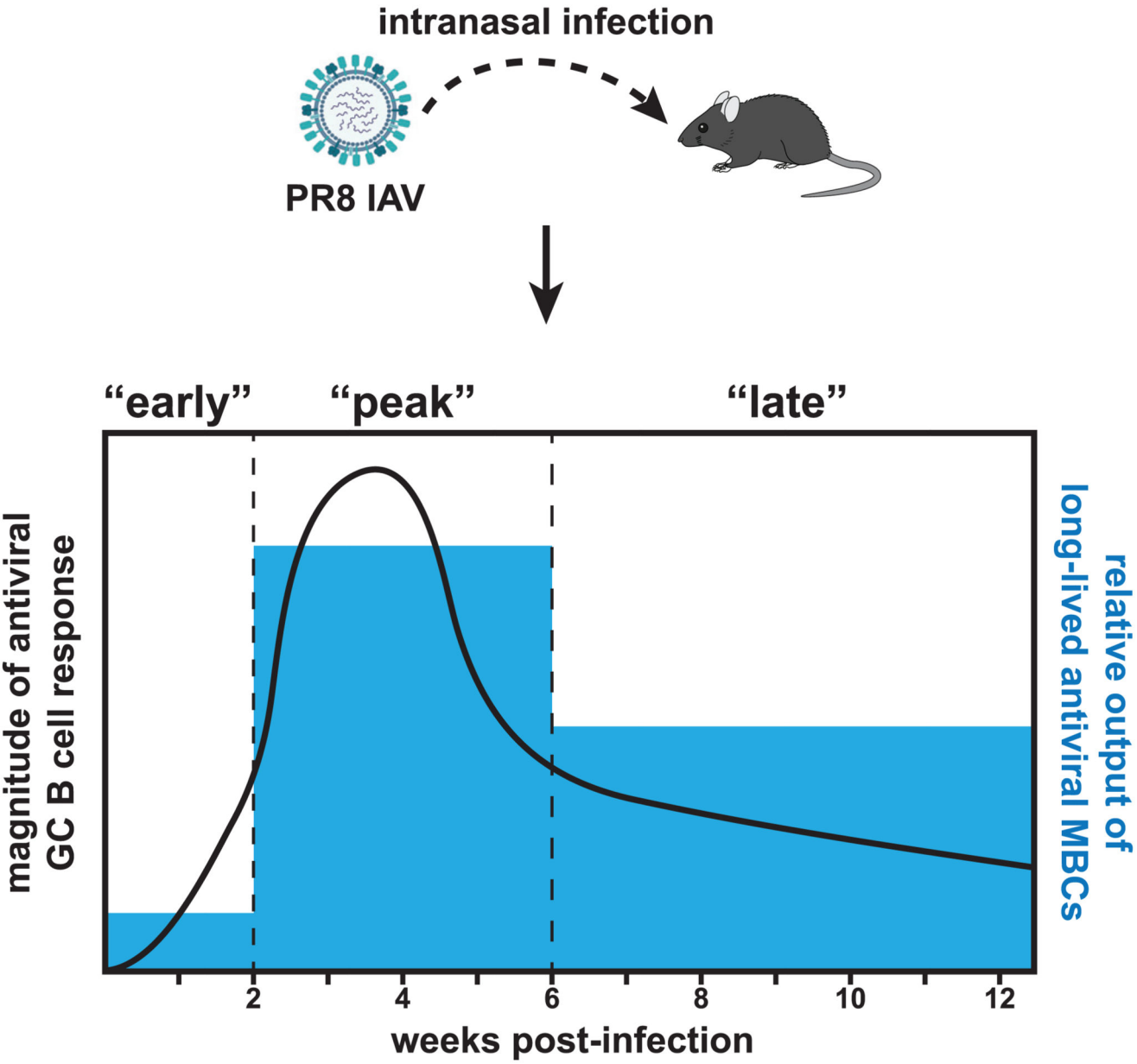

Graphical abstract.

Introduction

Upon exposure to viruses or vaccines, immunogen-activated B cells can differentiate into plasma cells (PCs), return to a naive-like resting state as memory B cells (MBCs), or enter a

germinal center (GC) reaction. Within GCs, B cells undergo somatic hypermutation (SHM)-based affinity maturation and selection for higher affinity clones that face similar cell fate decisions (Mesin et al., 2016). PCs selectively differentiate from higher-affinity GC B cells (Ise et al., 2018; Phan et al., 2006; Smith et al., 1997; Taylor et al., 2015); however, their terminal differentiation precludes expansion upon subsequent challenges. MBCs exhibit increased clonal diversity, which in conjunction with further somatic mutations and selection provides enormous flexibility to rapidly respond and adapt to homologous and heterologous challenges (Leach et al., 2019; Mesin et al., 2020; Purtha et al., 2011; Wong et al., 2020). Thus, PCs and MBCs perform complementary roles in providing antiviral immunity (Akkaya et al., 2020).

MBCs are inherently challenging to study. Present at low frequencies and not readily defined by unique cell surface markers, their study requires experiments spanning months. Transgenic hapten-specific B cell receptor (BCR) mouse models, adoptive transfer protocols and elegant studies using fluorescent protein immunizations helped surmount these challenges and established basic principles of MBC biology. However, fewer studies investigate anti-microbial MBC responses, in which polyclonal B cells experience vastly different immunogens and innate signals. The introduction of fluorescent pathogen-derived immunogens has enabled the tracking of microbe-specific polyclonal B cells and accelerated the understanding of MBC responses during infections (Frank et al., 2015; Krishnamurty et al., 2016; Onodera et al., 2012; Purtha et al., 2011; Wong et al., 2020).

Influenza A virus (IAV), a ubiquitous human virus that infects a significant fraction of humanity every year (Victora and Wilson, 2015), induces persistent GC responses (Adachi et al., 2015; Onodera et al., 2012; Rothaeusler and Baumgarth, 2010), although the temporal dynamics of antiviral GCs and MBC differentiation are largely uncharacterized. While MBCs are thought to predominantly differentiate early on during shorter-lived GC responses (Weisel et al., 2016), a major question is whether persistent GC responses adhere to a similar temporal regulation. The observations that severe acute respiratory syndrome coronavirus 2 (SARS-CoV-2) infection, as well as some vaccinations with replication-competent virus, induce a gradual increase in MBC BCR somatic mutations spanning many months suggest that MBCs continually differentiate from persistent GCs (Dugan et al., 2021; Gaebler et al., 2021; Matsuda et al., 2019; Sakharkar et al., 2021; Sokal et al., 2021; Wang et al., 2021). However, this hypothesis has never been formally tested. Furthermore, understanding the temporal regulation of MBCs has critical implications for the design of vaccination strategies that take full advantage of ongoing antibody affinity maturation within persistent GCs.

To comprehensively evaluate the humoral response to respiratory virus infection, we infected mice intranasally with IAV to generate an upper and lower airway infection, and examined the temporal dynamics of persistent GCs and MBC differentiation. Hemagglutinin-specific (HA^+) GCs can persist for well over 100 days within lung-draining mediastinal lymph nodes (mLNs), while splenic GCs dissolve after 6 weeks post-infection. Furthermore, HA^+ B cells are more frequent within mLN GCs and MBC compartments versus the spleen and undergo differential class switching dynamics, depending on the lymphoid organ. Persistent GCs continually differentiate HA^+ MBCs for at least 3 months

post-infection, and we estimate their peak output is on the order of 3 HA^+ MBCs per day. Lastly, single-cell genomic analysis of long-lived HA^+ MBCs revealed key gene products that may contribute to MBC longevity and self-renewal. Our findings uncover fundamental properties of persistent antiviral GC B cell responses and MBC differentiation, which have direct relevance to the development of optimal vaccination strategies against respiratory viruses such as IAV and SARS-CoV-2.

Results

Influenza infection induces persistent HA-specific GCs

To investigate the dynamics of the B cell response to viral infection, we infected mice intranasally with the highly mouse-adapted PR8 strain of influenza A virus, and analyzed B cell responses by flow cytometry spanning 182 days post-infection. To track IAV-specific B cells, we used a fluorescently labeled recombinant HA trimer (Whittle et al., 2014); HA is the immunodominant antigen following infection, comprising upward of 50% of the B cell response (Altman et al., 2018). To control for the specificity of HA staining, we infected mice with J1, a reassortant virus identical to PR8 aside from replacement with the H3 HA gene segment; antibodies to the widely divergent H1 and H3 HAs do not significantly cross-react (Frank et al., 2015; Palese, 1977) (Figures 1A and S1A).

GC responses in the lung-draining mLN peaked in frequency and absolute number at d21 post-infection and persisted through d154, while splenic GCs peaked at d14 and returned to uninfected control levels by d49 (Figures 1 B and S1B). We detected mLN HA^+ GCs from d7 to d154 post-infection, whereas splenic HA^+ GCs diminished to J1 control levels by d56 (Figures 1C and 1D). HA^+ GC B cells were present at low but consistent frequencies in both lymphoid organs early in the response. There was a sharp increase in average frequency at d21 in the mLN, after which up to 30% of mice contained GCs with >10% HA^+ B cells. Subsequently, the average frequency of HA^+ B cells within mLN GCs persisted between 5% and 10% through d77 post-infection, and then gradually declined (Figures 1C and 1D). GCs consist of light zone (LZ) and dark zone (DZ) regions (Mesin et al., 2016), leading us to test whether their frequencies fluctuate during a persistent GC response. We found that after d7, the proportion of DZ and LZ GC B cells remained relatively stable (Figure S1C). These data indicate that splenic and draining LN virus-specific GCs exhibit differential temporal regulation and enrichment for antigen-binding cells. The presence of HA^+ GCs well past 100 days post-infection suggests IAV antigen persistence in the mLN versus spleen, extending the intriguing finding that IAV-specific CD8 T cells are activated in the mLN of infected mice when adoptively transferred 60 days post-infection (Zammit et al., 2006).

Differential class-switching dynamics among splenic and mLN HA^+ B cells

To examine the kinetics of immunoglobulin heavy chain (*Igh*) class-switch recombination (CSR) following IAV infection, we measured the frequency of class-switched B cells in the mLN and spleen. The majority of mLN GC B cells had undergone CSR by d7 (Figure 2A), consistent with reports that CSR can begin before GC B cell differentiation (Roco et al., 2019), and by d28, mLN GC B cells were 90% class switched. Bulk GC and HA^+ B

cell CSR dynamics were similar in the mLN. In contrast, splenic HA^+ B cell CSR was markedly delayed early in the response (Figure 2A). Intriguingly, bulk splenic GC B cells were 60% class-switched at d10 versus 30% among HA^+ GC B cells. At d14 post-infection, splenic GCs contained more than twice as many IgG1 class-switched B cells versus any other isotype, whereas IgG2c was predominant in mLN GCs (Figures 2B and 2C). Despite the predominance of IgG1 class switching in overall splenic GCs, splenic HA^+ GC B cells were enriched for IgG2c and IgG2b, as found in the mLN (Figures 2B and 2C). These data suggest that splenic GCs contain B cells that undergo an early wave of IgG1 CSR (Figure 2D) that is temporally and qualitatively distinct from HA^+ B cell CSR. Early $IgG1^+$ CSR could be triggered by another IAV antigen or could be IAV antigen independent, and may be related to an early wave of natural killer (NK) T cell-derived interleukin-4 (IL-4) following viral infection (Gaya et al., 2018), as IL-4 activates the *Ighγ1* germline transcription required for IgG1 CSR (Yewdell and Chaudhuri, 2017).

HA^+ MBCs persist in mLNs for at least 6 months post infection

We next examined the temporal dynamics of HA^+ MBCs, defined as $HA^+CD38^+GL7^-IgD^-IgM^-B220^+$ live cells. We detected HA^+ MBCs in the mLN from d10 post-infection onward, whereas splenic HA^+ MBCs were detectable from d10 to d98, after which they did not exceed J1 control levels (Figures 3A–3C). In contrast to a previous report (Viant et al., 2020), antigen binding (HA^+) cells were enriched among bulk MBCs (Figure S2A), although this may reflect inherent differences in immunogens, or the concentration of antigen used to stain cells. As a proportion of resting class-switched cells, HA^+ MBCs were ~4-fold more frequent in the mLN than spleen, with a notable peak at d70. mLN HA^+ MBCs numbered in the hundreds and were present at 10-fold higher frequencies and numbers than J1 controls, whereas absolute numbers of splenic HA^+ MBCs were slightly higher, but only 2- to 3-fold more frequent than J1 controls (Figures 3B and 3C).

At d104–109 post-infection, mLN HA^+ MBCs were predominantly $IgG2c^+$ (41%), followed by $IgG2b^+$ (22%) and $IgG1^+$ (11%) (Figure 3D), reflecting the spectrum of HA^+ GC B cell CSR at d14 (30% $IgG2c^+$, 23% $IgG2b^+$, and 11% $IgG1^+$) (Figure 2C). We detected a low but significant frequency of IgM^+ HA^+ MBCs (defined as $HA^+CD38^+GL7^-IgM^+IgD^-B220^+$ live cells); however, their absolute numbers were 10-fold lower than class-switched HA^+ MBCs (Figure S2B). It is possible that they are recently activated naive B cells that have not yet upregulated GL7, or they were generated in a GC-independent pathway (Taylor et al., 2012).

Given the predominance of $IgG2c^+$ HA^+ MBCs (Figure 3D), the requirement for the transcription factor T-bet in IgG2c CSR (Peng et al., 2002), and the known role for T-bet in antiviral responses (Barnett et al., 2016; Mendoza et al., 2021), we used a reporter mouse in which tdTomato expression is driven from the endogenous *Tbx21* locus to assess T-bet expression in HA^+ MBCs (Figure S2C) (Levine et al., 2017). We found that 90% of HA^+ MBCs and GC B cells expressed T-bet at d84–85 post-infection, compared to 37% of naive B cells. Among $T\text{-}bet^+$ B cells, HA^+ MBCs exhibited the highest T-bet expression, followed by bulk MBCs and GC and naive B cells (Figures 3E and 3F). The uniformly high T-bet expression among HA^+ MBCs indicates that T-bet may play an important role in their

maintenance or function, augmenting the finding that B cell-intrinsic T-bet is required for the formation of antibody secreting cells upon secondary challenge (Stone et al., 2019).

Overall, these data indicate that first, HA^+ MBCs are preferentially enriched in the mLNs versus the spleen; second, that they persist in the mLNs for at least 182 days; and third, that the IgG isotype is not likely to bias HA^+ MBC differentiation from GCs, as HA^+ MBC BCR isotypes mirror d14 HA^+ GC B cell isotypes.

HA^+ MBCs continuously differentiate from persistent GCs

To assess the kinetics of MBC differentiation from persistent GCs, we added 5-ethynyl-2′-deoxyuridine (EdU) to the drinking water of PR8-infected mice during 3 distinct labeling windows: “early” (d0–14), “peak” (d14–42), and “late” (d42–88) (Figure 4A), and assessed EdU incorporation into HA^+ MBCs at d104-109 post-infection (Figure 4B). EdU is incorporated into the DNA of dividing cells; thus, MBCs that differentiate within each labeling window and become quiescent will retain incorporated EdU, which can be detected by flow cytometry. EdU labeling did not drastically affect the frequency or number of HA^+ MBCs (Figures S3A and S3B). Early window labeling resulted in 2% EdU^+ of mLN HA^+ MBCs, whereas peak and late labeling each resulted in ~30% EdU labeling (Figure 4C). Splenic HA^+ MBCs revealed a similar temporal regulation of differentiation (Figure S3C). Compared to bulk MBCs, HA^+ MBCs were enriched for EdU labeling across all windows in both organs (Figures S3D and S3E), indicating that either a large fraction of bulk MBCs had differentiated before IAV infection, HA^+ MBCs selectively persisted, or HA^+ MBCs were selectively retained within lymphoid organs, which are not mutually exclusive. To assess the longevity of HA^+ MBCs, we performed EdU labeling from d0 to d88, followed by a chase to d180. We found that 45% of HA^+ MBCs retained EdU (Figures 4D and S3F), indicating that a large fraction of long-lived HA^+ MBCs generated during the first 3 months post-infection persist with minimal cell division for at least 3 months.

To gauge the output of HA^+ MBC differentiation during each labeling window, we normalized the frequency of EdU positivity among HA^+ MBCs to the duration of each labeling window. This metric relates the percentage of total HA^+ MBCs differentiating per day, with the caveat that earlier differentiating HA^+ MBCs have more time to exit the LNs or to re-enter ongoing GCs. Thus, their output may be underrepresented at d104–109. We found that peak GCs output 0.94% of total HA^+ MBCs per day, while early and late GCs output 0.13% and 0.53%, respectively (Figure 4E). Given an average of 351 total HA^+ MBCs present within mLNs at d104–109 (Figure S3A), early, peak, and late GCs produce ~0.45, 3.3, and 1.9 of these HA^+ MBCs per day, respectively. Furthermore, given that mLNs and splenic GCs contain an average total of 20,000 HA^+ B cells throughout the peak labeling window (Figure 1C), and we estimate peak HA^+ MBC differentiation to be on the order of 1–10 HA^+ MBCs/day (to account for EdU^+ HA^+ MBCs not present within mLNs at d104–109), differentiation of a long-lived HA^+ MBC from peak GCs is approximately a 1 in 2,000–1 in 20,000/day event. These data indicate that long-lived HA^+ MBCs continually differentiate from persistent GCs, with the maximum output (MBCs/day) likely occurring during the peak of the GC response and diminishing thereafter.

Single-cell BCR and RNA sequencing of long-lived HA$^+$ MBCs

While recent studies have identified critical regulators of MBC differentiation (Laidlaw and Cyster, 2021), less is known about the requirements for MBC longevity; MBCs can persist for decades (Crotty et al., 2003), while naive B cells have an estimated half-life of 6 weeks (Fulcher and Basten, 1997). Factors such as BAFF and BCR signaling are required for MBC survival (Ackermann et al., 2015; Müller-Winkler et al., 2021); however, they are also required for the survival of mature naive B cells (Lam et al., 1997; Schiemann et al., 2001; Schneider et al., 2001). Thus, a key challenge is identifying specific factors that endow MBC longevity in comparison to shorter-lived but otherwise phenotypically similar naive B cells.

To this end, we performed single-cell BCR and transcriptome analyses of 1,326 mLN HA$^+$ MBCs and 5,421 naive B cells sorted at d109 post-infection (Figure S4A), a time point that contains a high proportion of bona fide long-lived HA$^+$ MBCs (Figures 4C and 4D). Unbiased clustering revealed that naive B cells clustered distinctly from HA$^+$ MBCs and were defined by the expression of *Ighm, Ighd, Fcer2a* (CD23), and *Sell* (CD62L) (Figures 5A–5D). In addition to expressing class-switched IgG BCRs, HA$^+$ MBCs were defined by the chemokine receptor *Cxcr3*, which was recently implicated in antiviral MBC biology (Oh et al., 2019; Stone et al., 2019), and *Zbtb20*, a transcription factor that regulates PC differentiation and longevity (Chevrier et al., 2014; Wang and Bhattacharya, 2014) (Figures 5B–5D). The top-ranked gene defining HA$^+$ MBCs was apolipoprotein E (*Apoe*), which was highly expressed by 91% of MBCs (Figures 5B, 5D, and S4B), and was recently found to define IgG2b$^+$ and IgG2c$^+$ MBCs in the spleen and bone marrow (Riedel et al., 2020) and HA$^+$ MBCs isolated at d7–28 post-IAV infection (Mathew et al., 2021). Intriguingly, ApoE expression is part of a transcriptional program shared among hematopoietic stem cells (HSCs) and memory T and B cells, suggesting a potential role in promoting self-renewal and/or longevity (Luckey et al., 2006). A small subset of HA$^+$ MBCs expressed detectable levels of the canonical MBC markers CD80, PD-L2, or CD73 (Figure 5D) (Tomayko et al., 2010). However, it is important to note that while nearly all HA$^+$ MBCs had high levels of T-bet expression as indicated by the *Tbx21*^{RFP} reporter (Figure S2C), only a small fraction of HA$^+$ MBCs expressed detectable T-bet via single-cell RNA (scRNA) transcriptome analysis (Figure S4B).

We found that 92% of HA$^+$ MBCs had somatically hypermutated *Igh* BCRs, indicating activation-induced cytidine deaminase expression and likely GC differentiation, while 8% had no detectable mutations, and thus may be GC-independent (Taylor et al., 2012) (Figure 5E). Among HA$^+$ MBCs, IgG2c$^+$ and IgG2b$^+$ cells had the highest average mutation rates (Figure 5F), and we identified 2 V genes, *Ighv14-2* and *Ighv1-63*, that were enriched 8.63-fold and 23.2-fold, respectively, relative to the naive B cell repertoire (Figure S4C). A previous study found *Ighv14-2* enriched among late GC B cells following HA immunization (Kuraoka et al., 2016); thus, this particular rearranged BCR may be useful for the development of transgenic HA-specific mouse models. These data identify several key gene products that have been implicated in either MBC function upon recall or longevity, and are thus prime candidates for future studies examining their role *in vivo* following viral infection.

Discussion

Unlike B cell responses to protein antigens in standard adjuvants, viral infections induce a vastly different innate immune response driven by cytokines and chemokines released by infected cells. The SARS-CoV-2 pandemic highlights the critical need for a better understanding of the factors leading to durable protective antibody responses following infection and vaccination. Here, we studied the unique features of the B cell response to IAV, another important human respiratory pathogen. We detected sizeable HA^+ GCs in the mLN up to 126 days post-infection, suggesting persistent viral antigen presentation. These data are consistent with the previous findings that while infectious IAV and viral RNA are undetectable in the mLNs past d10 post-infection, naive IAV-specific CD4 and CD8 T cells become activated in the mLNs of infected mice when adoptively transferred up to 30 and 60 days post-infection, respectively (Jelley-Gibbs et al., 2005; Kim et al., 2010; Zammit et al., 2006). The persistence of viral antigens is not unique to IAV; naive OT-I CD8 T cells become activated when adoptively transferred 45 days post-intranasal infection with vesicular stomatitis virus expressing Ova (VSV-Ova) (Turner et al., 2007), and VSV immunization is thought to induce persistent GCs associated with persistent viral antigens (Bachmann et al., 1996). However, antigen persistence is not an inevitable consequence of microbially induced lung inflammation, as intranasal infection with *Listeria monocytogenes* expressing Ova does not result in comparable OT-I CD8 T cell activation following adoptive transfer at d22 post-infection (Turner et al., 2007). Understanding whether antigen persistence is a unique feature of certain viruses and/or dependent on the route of infection is an important question for future studies.

How are viral antigens maintained for such long periods of time? Follicular dendritic cells (FDCs) play a central role in GC B cell positive selection by presenting antigens to LZ B cells assessing their own BCRs post-SHM (Heesters et al., 2016; Mesin et al., 2016). The ability of FDCs to internalize complement-coated immune complexes to nondegradative endosomal compartments, which can then undergo multiple rounds of surface recycling (Heesters et al., 2013), make them a prime candidate to store persistent viral antigens. FDCs are generally thought to be able to retain intact antigen for weeks to many months, although experimentally validating the limits of FDC antigen retention has been a major challenge (Heesters et al., 2014; Mandel et al., 1980; Tew and Mandel, 1979). Our data, in conjunction with the current model for GC B cell positive selection, indicate that FDCs may retain native HA well past 100 days post-infection.

While the presence of HA binding GC B cells suggests the persistence of native HA, a previous study found that a large fraction of GC B cells responding to immunization with recombinant HA do not display any detectable binding to native HA, yet underwent both SHM and selection (Kuraoka et al., 2016). The authors hypothesized that these GC B cells recognized non-native HA conformations, or “dark antigens,” which could be exposed via degradation or other processes. Given the potential for persisting viral antigens to transform over the course of 100 days post-infection, the possibility of dark antigens arising within persistent GCs as native viral antigens degrade is intriguing. We observe that the average frequency of HA^+ GC B cells gradually decreases from d77-126, while the frequency and absolute number of total GC B cells remain relatively constant. The rise of dark antigens and

the increased clonal diversity observed in late GCs may provide the benefit of an expanded repertoire to combat future heterologous infections (Kuraoka et al., 2016) or may be useless or even deleterious if denatured immunogens induce self-reactive antibodies.

The landmark finding that MBCs predominantly differentiate from early GCs (Weisel et al., 2016) raised the major question of whether persistent GCs follow a similar temporal regulation. While we found that hundreds of HA^+ MBCs had differentiated by d10 or d14 in both the spleen and the mLN, the early (d0–14) EdU pulse window accounted for only 2% of the mLN HA^+ MBCs at d109 post-infection, suggesting that long-lived HA^+ MBCs predominantly differentiate after the first 2 weeks post-infection. We observed that the maximal output of long-lived HA^+ MBCs (3.3 cells/day) corresponded with the peak of the mLN GC response (d14–42); this was 7.3-fold greater than the early (d0–14) long-lived HA^+ MBC output (0.45 cells/day). Notably, the output during the late (d42–88) EdU pulse window (1.9 cells/day) was only 1.7-fold less than the peak window, and peak and late pulse windows accounted for virtually identical fractions of mLN HA^+ MBCs at d109 post-infection. These data indicate that while HA^+ MBCs continually differentiate from persistent GCs, the majority of long-lived HA^+ MBCs predominantly differentiate after the first 2 weeks post-infection, and peak and late GCs contribute equal fractions of HA^+ MBCs to the long-lived pool. Furthermore, the long temporal window of differentiation may facilitate the time-dependent differentiation of MBCs with different functions and capabilities.

Three findings support the relevance of these data to human responses to vaccination and infection. First, fine-needle aspiration of draining LNs revealed persistent GCs in a subset of quadrivalent inactivated IAV vaccine trial participants (Turner et al., 2020), as well as following SARS-CoV-2 mRNA-based vaccination (Turner et al., 2021). Second, vaccination with an HA-expressing replication-competent adenovirus induced MBC responses that continuously evolved over the course of many months (Matsuda et al., 2019). Third, infection with SARS-CoV-2 induces GCs that can persist for 6 months (Poon et al., 2021), as well as a gradual increase in MBC BCR somatic hypermutation spanning 12 months post-infection (Gaebler et al., 2021; Sakharkar et al., 2021; Sokal et al., 2021; Wang et al., 2021). These results suggest the continuous differentiation of MBCs from persistent GCs in humans, and highlight the importance of reconsidering the timing of boosting immunizations following vaccination or infection (Matsuda et al., 2019). In light of the continuous differentiation of MBCs, boosting immunizations typically administered 1–2 months post-vaccination (or post-infection) cannot access fully matured MBC responses that are driven by persistent GCs, and may be delayed or perhaps boosted with a third vaccination.

Our EdU pulse-chase analysis estimated the occurrence of long-lived HA^+ MBC differentiation from peak GCs to be a 1 in 2,000–1 in 20,000 event. This underscores the rarity of long-lived antiviral MBC differentiation and highlights the importance of investigating the mechanisms that regulate this process. Recent studies have implicated numerous factors in the regulation of MBC differentiation, including the transcription factors Bach2 and Hhex (Laidlaw et al., 2020; Shinnakasu et al., 2016), IL-9 signaling molecules (Takatsuka et al., 2018; Wang et al., 2017), the chemokine receptor Ccr6 (Suan et al., 2017), and mammalian target of rapamycin complex 1 (mTORC1) signaling and

the tyrosine kinase ligand Ephrin-B1 (Inoue et al., 2021; Laidlaw et al., 2017). However, identifying factors with differential requirements in MBC and naive B cell survival remains a challenge. To this end, we performed scRNA BCR and transcriptome analyses on sorted, long-lived HA^+ MBCs mixed with contemporaneous naive B cells. With limited exceptions, previous MBC scRNA analyses have been limited to homeostatic MBC populations or were performed at earlier time points post-infection, likely due to the technical challenges in sorting small numbers of cells after long periods of time. Our rigorous, quantitative temporal analysis, J1 negative controls, and EdU pulse-chase data ensured that we were sorting bona fide long-lived HA^+ MBCs, and provided the guidance to retrieve sufficient cell numbers for analysis at d109 post-infection. Given that we pooled cells from 2 independent experiments containing 62 total mice, the relative homogeneity among HA^+ MBCs suggests that this population is reliably generated following intranasal infection, despite any differences in viral clearance, persistent GC dynamics, or other biological variables that may arise within individual mice.

We identified ApoE as the foremost gene differentiating long-lived HA^+ MBCs from naive B cells; ApoE was highly expressed among virtually all HA^+ MBCs. Strikingly, ApoE was previously identified as a component of a transcriptional program shared among HSCs, memory T cells, and MBCs, indicating a potential role in self-renewal and/or longevity (Luckey et al., 2006). While MBCs can persist for decades (Crotty et al., 2003), there is currently no consensus regarding their requirements for homeostatic cell division or self-renewal. Pulse-chase experiments using a doxycycline-inducible H2B-GFP reporter found that 4-hydroxy-3-nitrophenylacetyl (NP)-binding MBCs persist without measurable cell division for at least 300 days post-immunization (Jones et al., 2015). However, other data hint that MBCs may undergo some low level of homeostatic proliferation (Schittek and Rajewsky, 1990), similar to the landmark finding that yellow fever virus-specific memory CD8 T cells have a doubling half-time of 493 days (Akondy et al., 2017). Further studies of ApoE and the other gene products identified herein will, it is hoped, illuminate the molecular mechanisms underlying the remarkable longevity of MBCs and their accelerated function upon recall, both of which are critical to developing effective vaccination strategies.

Limitations of the study

There are some key limitations to the interpretations of the data presented here. First, we defined MBCs as resting, class-switched, HA-binding cells. However, unbiased fate mapping of MBCs has revealed that, under certain experimental conditions, a significant fraction of fate-mapped MBCs can be characterized as antigen binding only under conditions of increased valency and not via conventional flow cytometry staining (Viant et al., 2020). Given that our study defines HA binding via flow cytometry, we do not capture the dynamics of these lower-avidity MBCs. Second, enriching for antigen-binding cells with magnetic beads coupled to HA may enhance the detection of HA^+ MBCs relative to J1 and PBS control levels. Previous studies have used this strategy to enrich for phycoerythrin (PE)- and plasmodium-specific MBCs (Krishnamurty et al., 2016; Pape et al., 2011).

Star⋆Methods

Key Resources Table

REAGENT or RESOURCE	SOURCE	IDENTIFIER
Antibodies		
BV786 Rat Anti-Mouse CD45R/B220	BD Biosciences	Cat#: 563894; RRID: AB_2738472
BUV737 Rat Anti-Mouse CD45R/B220	BD Biosciences	Cat#: 612838
FITC Rat Anti-Mouse CD45R/B220	BD Biosciences	Cat# 553087, RRID:AB_394617
BUV395 Rat Anti-Mouse CD45R/B220	BD Biosciences	Cat# 563793, RRID:AB_2738427
BUV395 Rat Anti-Mouse IgM	BD Biosciences	Cat#: 743329; RRID: AB_2741430
BV786 Rat Anti-Mouse IgM	BD Biosciences	Cat#: 743328; RRID: AB_2741429
IgM Monoclonal Antibody (II/41), APC-eFluor 780, eBioscience	Thermo Fisher Scientific	Cat# 47-5790-80, RRID:AB_2573983
BV510 Rat Anti-Mouse IgG1	BD Biosciences	Cat# 742476; RRID: AB_2740810
BV786 Rat Anti-Mouse IgG1	BD Biosciences	Cat# 742480, RRID:AB_2740814
PE-Cy7 Hamster Anti-Mouse CD95	BD Biosciences	Cat#: 557653; RRID: AB_396768
GL7 Monoclonal Antibody (GL-7 (GL7)), eFluor 450, eBioscience	Thermo Fisher Scientific	Cat#: 48-5902-80; RRID: AB_10854881
CD38 Monoclonal Antibody (90), Alexa Fluor 700, eBioscience	Thermo Fisher Scientific	Cat#: 56-0381-82; RRID:AB_657740
Goat Anti-Mouse IgG2c, Human ads-FITC	Southern Biotech	Cat#: 1079-02; RRID: AB_2794465
CD86 (B7-2) Monoclonal Antibody (GL1), PE, eBioscience	Thermo Fisher Scientific	Cat#: 12-0862-82; RRID: AB_465768
BUV395 Rat Anti-Mouse CD86	BD Biosciences	Cat#: 564199; RRID: AB_2738664
Goat Anti-Mouse IgG2b, Human ads-APC/CY7	Southern Biotech	Cat#: 1090-19; RRID: AB_2794530
Brilliant Violet 711 anti-mouse IgD	BioLegend	Cat#: 405731; RRID: AB_2563342
CD184 (CXCR4) Monoclonal Antibody (2B11), PerCP-eFluor 710, eBioscience	Thermo Fisher Scientific	Cat#: 46-9991-82; RRID: AB_10670489
CD138 Rat anti-Mouse, BUV737, Clone: 281-2	BD Biosciences	Cat# 564430, RRID:AB_2738805
Purified Rat Anti-Mouse CD16/CD32 (Mouse BD Fc Block)	BD Biosciences	Cat#: 553142; RRID: AB_394657
APC Streptavidin	BioLegend	Cat#: 405207
Bacterial and virus strains		
Influenza A/Puerto Rico/8/34 (PR8) mouse adapted influenza strain, grown in 10 day-old embryonated chicken eggs	Yewdell laboratory, (NIAID, NIH)	N/A
J1, PR8 reassortant virus, mouse adapted influenza strain, grown in 10 day-old embryonated chicken eggs	Yewdell laboratory, (NIAID, NIH)	N/A
Chemicals, peptides, and recombinant proteins		
2′-Deoxy-5-ethynyluridine	Carbosynth	Cat#: NE08701
Recombinant PR8 HA-biotin	Chaudhuri Lab	NA
PEI MAX	Polysciences, Inc.	Cat#: 24765-1
Critical commercial assays		
DMEM, high glucose	GIBCO	Cat#: 11965118

REAGENT or RESOURCE	SOURCE	IDENTIFIER
FreeStyle 293 Expression Medium	Thermo Fisher Scientific	Cat#: 12338018
Zombie Red Fixable Viability Kit	BioLegend	Cat#: 423110
CountBright Absolute Counting Beads	Thermo Fisher Scientific	Cat#: C36950
Click-iT EdU Alexa Fluor 488 Flow Cytometry Assay Kit	Thermo Fisher Scientific	Cat#: C10425
BirA500: BirA biotin-protein ligase standard reaction kit	Avidity	Cat#: BirA500
Amicon® Ultra-15 Centrifugal Filter Unit	EMD Millipore	Cat#: UFC910024
HisTrap excel	Cytiva Life Sciences	Cat#: 17371205
Superdex 200 Increase 10/300 GL gel filtration column	Cytiva Life Sciences	Cat#: 28990944
Chromium Single Cell A Chip Kit	10X Genomics	Cat#: 120236
Chromium Single Cell 5′ Library and Gel Bead Kit	10X Genomics	Cat#: 1000006
Chromium Single Cell 5′ Library Construction Kit	10X Genomics	Cat#: 1000020
Chromium Single Cell V(D)J Enrichment Kit for Mouse B Cells	10X Genomics	Cat#: 1000072
Chromium i7 Multiplex Kit	10X Genomics	Cat#: 120262
Chromium i7 Multiplex Kit N, Set A	10X Genomics	Cat#: 1000084
Deposited data		
Single-cell BCR and RNA-seq	This paper	GSE181009, https://www.ncbi.nlm.nih.gov/geo/query/acc.cgi?acc=GSE181009
Experimental models: cell lines		
FreeStyle 293-F Cells	Thermo Fisher Scientific	Cat#: R79007
Madin Darby Canine Kidney Cell Line	Yewdell laboratory, (NIAID, NIH)	N/A
Experimental models: organisms/strains		
Mouse: *Tbx21*^{RFP}	A. Rudensky (Levine et al., 2017)	N/A
Mouse: C57BL6/J	The Jackson Laboratory	JAX: 000664
Recombinant DNA		
PR8 HA	McDermott laboratory (VRC, NIAID,NIH)	VRC 3687
Software and algorithms		
10x Genomics Cell Ranger (v4.0.0)	10x Genomics	https://support.10xgenomics.com/single-cell-gene-expression/
R Software v4.0.2	CRAN	https://www.r-project.org/
Seurat R package (v3.2.2)	Stuart etal., 2019	https://cran.r-project.org/web/packages/Seurat/index.html
Immcantation SHazaM & Alakazam Packages v1.0.2	Gupta etal., 2015	http://immcantation.readthedocs.io
ggPlot2	(Wickham, 2009)	https://ggplot2.tidyverse.org/
Prism	Graphpad	RRID: SCR 002798
FlowJo	TreeStar	RRID: SCR_008520
Excel	Microsoft	RRID: SCR 016137

REAGENT or RESOURCE	SOURCE	IDENTIFIER
Illustrator	Adobe	RRID: SCR_010279

Resource Availability

Lead contact—Further information and requests for resources and reagents should be directed to and will be fulfilled by the lead contact, Jayanta Chaudhuri, (chaudhuj@mskcc.org).

Materials availability—All materials generated in this study are available upon request with a completed Materials Transfer Agreement.

Experimental Model and Subject Details

Mice—All mice were bred and housed under specific pathogen-free conditions and handled in accordance with the guidelines for animal care of MSKCC Research Animal Resource Center and the Institutional Animal Care and Use Committee (IACUC). Mouse strains include C57BL/6J (WT) and *Tbx21*^{RFP} (Levine et al., 2017). Experiments were conducted using 8-14 week old male and female mice as indicated in the figure legends. *Tbx21*^{RFP} mice were provided by Alexander Rudensky, C57BL/6J mice were ordered from The Jackson Laboratory.

Cell lines—Madin-Darby Canine Kidney (MDCK) cells were cultured in DMEM (11965118, GIBCO) supplemented with 10% heat-inactivated FBS and 1% Pen-Strep (400-109, Gemini) under 5% CO_2 atmosphere at 37°C. FreeStyle 293-F cells were cultured in FreeStyle 293 Expression Medium (12338018, ThermoFisher Scientific) in sterile polycarbonate Erlenmeyer flasks under 8% CO_2 atmosphere at 37°C in an orbital shaker (135 rpm).

Influenza viruses—10 day-old embryonated chicken eggs were inoculated with 10^5 $TCID_{50}$ of Influenza A/Puerto Rico/8/34 (PR8) or J1, and viruses were grown for 48 h at 35°C and 55% humidity with gentle rotation. Eggs were chilled at 4°C for several hours prior to harvesting allantoic fluid, which was then clarified by centrifugation at 3,000 g for 15 min, aliquoted and stored at −80°C.

Method Details

Influenza infections—For intranasal infections, mice were anesthetized with 3% isofluorane and nasally inoculated with 50 $TCID_{50}$ of PR8 or J1 diluted in PBS plus 0.1% BSA (Sigma, A2153). $TCID_{50}$ values for viral stocks were determined by scoring cytopathic effects of infected MDCK cells. Briefly, 100 μL of MDCK cells were seeded at 4×10^5 cells/mL in a 96-well flat-bottom plate, and cultured overnight under 5% CO_2 atmosphere at 37°C. The following day, MDCK cells were washed twice with 200 μL of $TCID_{50}$ media (serum free MEM plus non-essential amino acids, 1 mM sodium pyruvate, 1.5 g/L sodium bicarbonate, 1 mM HEPES, 1 μg/mL TPCK treated trypsin (T1426, Sigma) and 1% Pen-Strep (400-109, Gemini)) per well, after which 180 μL of $TCID_{50}$ media was added

per well. 20 uL of PR8 or J1 viral stocks were then added to the first well (1:10 dilution) in quadruplicate, and 1:10 serial dilutions were performed from row 1 to row 11, leaving row 12 as a no virus control. Cells were cultured for 72-96 h under 5% CO_2 atmosphere at 37°C, after which the number of wells displaying cytopathic effects of viral infection at each dilution were recorded, and $TCID_{50}$ values were calculated using the Reed and Muench method.

Flow cytometry and cell sorting—Single-cell suspensions were prepared from mouse lymph nodes and spleen by mashing through a 70 μm cell strainer (352350, Corning). Single-cell suspensions from the spleen were resuspended in 2 mLs of red blood cell lysis buffer (150 mM NH_4Cl, 10 mM $KHCO_3$, 0.1 mM EDTA) for 5 min at 25°C, followed by neutralization with B cell media (RPM1 1640 plus L-Glutamine (11875, GIBCO), supplemented with 15% FBS, 1% Pen-Strep (400-109, Gemini), 55 μM β-Mercaptoethanol (21985023, GIBCO), and 2 mM L-Glutamine). For the PR8 time-course stain, PR8 HA^+ MBC sorting stain and PR8 T-bet stain, approximately 5-10 × 10^6 cells were washed once with 250 μL PBS, stained with Zombie Red fixable viability dye (423109, BioLegend, 1:500) or Ghost Dye Violet 510 (13-0870, Tonbo Bio-sciences, 1:1,000) for 15 min at 25°C in 200 μL in the dark, washed once with 250 μL FACS buffer (PBS + 2.5% FBS), stained with rat anti-mouse CD16/CD32 Fc Block (553142, BD Biosciences, 1:50) for 5 min at 25°C in 100 μL in the dark, and washed once with 250 μL FACS buffer before surface staining.

The following antibodies were used in various staining panels: B220-BV786 (563894, BD Biosciences), B220-BUV737 (612838, BD Biosciences), B220-FITC (553088, BD Biosciences), B220-BUV395 (563793, BD Biosciences), IgM-BUV395 (743329, BD Biosciences), IgM-BV786 (743328, BD Biosciences), IgM-APC-Cy7 (47-5790, eBioscience), IgG2b-APC-Cy7 (1090-19, Southern Biotech), IgG1-BV510 (742476, BD Biosciences), IgG1-BV786 (742480, BD Biosciences), Fas-PE-Cy7 (557653, BD Biosciences), GL7-eFluor 450 (48-5902-80, eBioscience), CD38-AF700 (56-0381-82, eBioscience), IgG2c-FITC (1079-02, Southern Biotech), CD86-PE (12-0862-82, eBioscience), CD86-BUV395 (564199, BD Biosciences), IgD-BV711 (405731, BioLegend), CXCR4-PerCP-eFluor 710 (46-9991-82, eBioscience), biotinylated HA trimer (recombinant protein produced in house), CD138-BUV737 (564430, BD Biosciences), streptavidin-APC (405207, BioLegend).

The staining panels and antibody dilutions used were as follows:

PR8 time-course stain: B220-BV786 (1:750), IgM-BUV395 (1:750), IgG2b-APC-Cy7 (1:150), IgG1-BV510 (1:750), Fas-PE-Cy7 (1:750), GL7-eFluor 450 (1:750), CD38-AF700 (1:750), IgG2c-FITC (1:200), CD86-PE (1:5,000), IgD-BV711 (1:750), CXCR4-PerCP-eFluor 710 (1:250), biotinylated HA trimer (concentration = 2.6 nM), streptavidin-APC (1:1652).

PR8 EdU stain: IgM-BV786 (1:750), CD86-BUV395 (1:4000), IgG2b-APC-Cy7 (1:150), IgG1-BV510 (1:750), IgG2c-PE (1:150), Fas-PE-Cy7 (:750), GL7-eFluor 450 (1:750), CD38-AF700 (1:750), IgD-BV711 (1:750), CXCR4-PerCP-eFluor 710

(1:250), B220-BUV737 (1:750), biotinylated HA trimer (final concentration = 8 nM), streptavidin-APC (1:542).

PR8 HA^+ MBC sorting stain: IgM-APC-Cy7 (1:750), Fas-PE-Cy7 (1:750), GL7-eFluor 450 (1:750), CD38-AF700 (1:750), IgD-BV711 (1:750), B220-FITC (1:750), biotinylated HA trimer (final concentration = 22.9 nM), streptavidin-APC (1:190).

PR8 T-bet stain: IgG1-BV786 (1:500), IgM-BUV395 (1:750), IgG2b-APC-Cy7 (1:150), Fas-PE-Cy7 (1:750), GL7-eFluor 450 (1:750), CD38-AF700 (1:750), IgG2c-FITC (1:200), IgD-BV711 (1:750), B220-BUV737 (1:750), biotinylated HA trimer (final concentration = 2.6 nM), streptavidin-APC (1:1652).

For the PR8 time-course stain, PR8 HA^+ MBC sorting stain and PR8 T-bet stain, surface antibodies were stained for 1 h at 4°C in 100 μL in the dark. Cells were washed 3X with 250 μL FACS buffer, stained with streptavidin-APC for 30 min at 4°C in 100 μL in the dark, washed 3X with FACS buffer, and resuspended in 135 μL FACS buffer. 15 μL of CountBright Absolute Counting Beads (C36950, ThermoFisher) were added prior to analysis on a flow cytometer, aside from samples used for cell sorting.

Data was acquired using an LSR II flow cytometer (BD Biosciences), and analyzed using FlowJo software (version 9.9). HA^+ memory B cells and naive B cells were sorted using a BDFACS Aria II (BD Biosciences), and analyzed post-sort for purity using an LSR II.

EdU labeling and detection—2′-Deoxy-5-ethynyluridine (EdU) (NE08701, Carbosynth) was added to the drinking water of mice at a final concentration of 0.5 mg/mL during the indicated labeling windows, and the drinking water was changed every 4 days. Lymph nodes and spleen were processed as detailed above, and the Click-iT EdU Alexa Fluor 488 flow cytometry assay kit (C10425, Invitrogen) was used to detect EdU incorporation according to the manufacturers protocol. Briefly, following Zombie Red fixable viability dye and Fc block staining, surface antibodies were stained for 1 h at 4°C in 100 μL in the dark, aside from Fas-PE-Cy7 and IgG2c-PE (see PR8 EdU stain above). Cells were washed 3X with 250 μL FACS buffer, stained with streptavidin-APC for 30 min at 4°C in 100 μL in the dark, washed 2X with 250 mL FACS buffer, and washed 2X with 250 μL PBS^+ 0.1% BSA (Sigma, A2153). Cells were then fixed with 4% paraformaldehyde in PBS for 15 min at 25°C in 100 μL in the dark, washed 2X with 250 μL PBS + 0.1% BSA (Sigma, A2153), and permeabilized by resuspending in 100 μL of saponin-based permeabilization and wash reagent for 15 min at 25°C in the dark. Cells were then spun down and resuspended in 200 μL of the Click-iT cocktail, incubated at 25°C for 30 min in the dark, washed 2X with 250 μL of saponin-based permeabilization and wash reagent, washed 2X with 250 μL FACS buffer, and stained with Fas-PE-Cy7 and IgG2c-PE for 30 min at 4°C in 100 μL in the dark. Cells were then washed 2X with 250 μL FACS buffer, resuspended in 135 μL FACS buffer, and 15 μL of CountBright Absolute Counting Beads (C36950, ThermoFisher) were added prior to analysis on a flow cytometer.

PR8 HA prep—The VRC 3687 plasmid for recombinant PR8 HA expression was a kind gift from Adrian McDermott to the Chaudhuri Lab. PR8 HA was expressed and purified as previously described (Whittle et al., 2014). Briefly, 293F cells were cultured in FreeStyle

293 Expression Medium (12338018, ThermoFisher Scientific) in sterile polycarbonate Erlenmeyer flasks at 37°C and under 8% CO_2 atmosphere, and diluted to a concentration of 1×10^6 cells/mL prior to transfection. Cells were transfected with 100 μg of PR8 HA plasmid mixed with 400 μg of PEI MAX (24765-1, Polysciences, Inc.) per 100mLs of culture, and cultured for 5 days. The supernatant was collected by centrifuging cells at 4000 x g, and loaded on a HisTrap excel column (17371205, GE) equilibrated in 20 mM sodium phosphate pH 7.4, 0.5 M NaCl. Columns were washed with 20 column volumes (CV) of wash buffer (20 mM sodium phosphate pH 7.4, 0.5 M NaCl, 10 mM imidazole), and eluted with 5 CV of elution buffer (20 mM sodium phosphate pH 7.4, 0.5 M NaCl, 500 mM imidazole) using an AKTA FPLC (Amersham Biosciences). The elute was dialyzed into PBS, concentrated using an Amicon 100 kDa filter (UFC910024, Millipore), and loaded on a Superdex 200 Increase 10/300 GL column (28990944, GE) equilibrated in PBS, using an AKTA FPLC. Fractions corresponding to trimeric HA were pooled, concentrated and buffer exchanged into Tris pH 8.0 using an Amicon 100 kDa filter in preparation for biotinylation. Purified HA was biotinylated using a BirA500 biotin-protein ligase standard reaction kit (BirA500, Avidity) according to the manufacturer's protocol. Biotinylated HA was buffer exchanged into PBS and concentrated to 2 mg/mL using an Amicon 100 kDa and stored at –80°C until use.

Single-cell RNA sequencing analyses—In two independent experiments, 30-32 mice were infected intranasally with 50 $TCID_{50}$ PR8, and hemagglutinin-specific (HA^+) memory B cells (MBCs) and naive B cells were sorted from combined mediastinal lymph nodes at d109 post-infection. For each experiment, 50,000-60,000 sorted naive B cells were mixed with 15,000-16,000 sorted HA^+ MBCs, and resuspended at a final concentration of approximately 1,000 cells per μL. 5 μL of this mixture was taken and analyzed using flow cytometry as the 'post-sort' fraction, and the remaining cells were used for Chromium Single Cell 5′ library construction and V(D)J enrichment (10X Genomics).

Single-cell RNA sequencing data were generated using standard 10X and Illumina techniques. Namely, Gel Bead-In-EMulsions were formed using the Chromium Single Cell A Chip Kit (PN-120236) and barcoded with the Chromium Single Cell 5' Library & Gel Bead Kit (PN-1000006). Libraries were generated with the Chromium Single Cell 5′ Library Construction Kit (PN-1000020), with B cell receptor codes enriched using the Chromium Single Cell V(D)J Enrichment Kit for Mouse B Cells (PN-1000072). Combinatorial libraries were annotated using the Chromium i7 Multiplex Kit (PN-120262) and Chromium i7 Multiplex Kit N, Set A, (PN-1000084) prior to standard Illumina sequencing using a Novaseq (Illumina).

Gene expression feature barcode matrices were generated by the cellranger v4.0.0 pipeline, mapped to the mm 10 mouse genome, and loaded into R Software v4.0.2. We did not observe batch effects in the two replicates, so their barcode matrices were aggregated and analyzed together using Seurat v3.2.2 (Stuart et al., 2019). Standard quality control removed genes expressed in fewer than 3 cells and removed cells with more than 7% of mitochondrial genes, less than 800 features, or unique feature counts less than 400 or more than 2500. This yielded 7,033 cells for downstream analysis. The data was normalized, and the 2,000 most variable genes were selected. The top nine principal components were used for unsupervised

clustering and the data was visualized in two-dimensional space using uniform manifold approximation and projection (UMAP) with a resolution of 0.15. Differentially expressed genes were identified between the resultant clusters using the default settings of Find All Markers and a log fold change cut-off of 0.3.

The V(D)J data was processed using the cellranger v4.0.0 vdj pipeline and the aggregated outputs from the two replicate experiments were analyzed with the Immcantation toolbox (http://immcantation.readthedocs.io). V(D)J assignment based on the mouse IMGT and IgBLAST reference databases was carried out using the Change-O tool. After removing cells with non-productive V-J heavy chain spanning pairs and an unknown heavy chain isotype, the pipeline yielded 7006 unique V(D)J barcodes. The V(D)J sequencing data captured 1061 out of the 1327 "HA^+ MBCs" (79.95%) and 4936 out of the 5524 "naïve B Cells" (89.3%) transcriptome barcodes. The SHM load was quantified with the SHazaM Immcantation package v1.0.2. (Gupta et al., 2015), and the observedMutations function was applied to the entire heavy chain sequence. The V gene usage was analyzed using the Alakazam Immcantation package v1.0.2 (Gupta et al., 2015). The AddMetaData Seurat function was used to integrate the SHM and BCR isotype data into the Seurat object. All visualizations were done with the ggplot2 R package v3.3.3 (Wickham, 2009).

Quantification and Statistical Analysis

All statistical analyses were performed with GraphPad Prism 9 (GraphPad Software, Inc), with the exception of scRNA sequencing analyses, which were performed using R software (v4.0.2). Flow cytometry data was analyzed using FloJo software (version 9.9). Graphs were edited using GraphPad Prism 9, and graph titles and axes labels were edited using Adobe Illustrator CS6. All graphs depict all data collected from all performed experiments, with the following exception: samples containing low counts of HA^+ B cells (< 20 cells) were omitted from the quantification of frequencies within HA^+ B cells, and data shown in Figure 2A does not include splenic HA^+ GC B cell time points beyond d49, as the majority of samples had low counts of HA^+ B cells (< 20 cells). Details on the statistical analyses performed in this study can be found in the figure legends.

Supplementary Material

Refer to Web version on PubMed Central for supplementary material.

Acknowledgments

W.T.Y. was supported by a Special Fellow award from the Leukemia & Lymphoma Society, a Ludwig Center Basic and Translational Immunology Postdoctoral Award, and a NIH T32 training grant (CA009149); A.M. was supported by a Ludwig Center Basic and Translational Immunology Post-doctoral Award and a Bristol-Myers Squibb Fellowship from the Cancer Research Institute; A.J.M. was supported by a National Cancer Institute predoctoral fellowship (F31 CA254325-01); D.A. was supported by the European Research Council Starting Grant (B-DOMINANCE, grant no. 850638), the Swedish Research Council (grant no. 2017-01439), and the Institute of Biomedicine at the University of Gothenburg; J.W.Y. was supported by the DIR, NIAID, Bethesda, MD; J.C. was supported by grants from the NIH (R01AI072194, R01AI124186, R56AI072194, U54CA137788, and P30CA008748), the Starr Cancer Research Foundation, the Ludwig Center for Cancer Immunotherapy, MSKCC Functional Genomics, and the Geoffrey Beene Cancer Center. We acknowledge the use of the Single Cell Research Initiative at MSKCC. We thank A. Bravo for help with maintenance of the mouse colony. We thank all of the members of the Chaudhuri lab for helpful discussions and feedback. We thank Adrian McDermott for providing HA

plasmids and guidance on their purification. We thank Alexander Rudensky for providing *Tbx21*^{RFP} mice. Some images in the graphical abstract were created with BioRender.com.

Data and code availability

- Single-cell BCR and RNA-seq data have been deposited at the Gene Expression Omnibus repository and are publicly available as of the date of publication. Accession numbers are listed in the Key resources table.
- This paper does not report original code.
- Any additional information required to reanalyze the data reported in this paper is available from the lead contact upon request.

References

Ackermann JA, Nys J, Schweighoffer E, McCleary S, Smithers N, Tybulewicz VL. Syk tyrosine kinase is critical for B cell antibody responses and memory B cell survival. J Immunol. 2015; 194: 4650–4656. [PubMed: 25862820]

Adachi Y, Onodera T, Yamada Y, Daio R, Tsuiji M, Inoue T, Kobayashi K, Kurosaki T, Ato M, Takahashi Y. Distinct germinal center selection at local sites shapes memory B cell response to viral escape. J Exp Med. 2015; 212: 1709–1723. [PubMed: 26324444]

Akkaya M, Kwak K, Pierce SK. B cell memory: building two walls of protection against pathogens. Nat Rev Immunol. 2020; 20: 229–238. [PubMed: 31836872]

Akondy RS, Fitch M, Edupuganti S, Yang S, Kissick HT, Li KW, Youngblood BA, Abdelsamed HA, McGuire DJ, Cohen KW, et al. Origin and differentiation of human memory CD8 T cells after vaccination. Nature. 2017; 552: 362–367. [PubMed: 29236685]

Altman MO, Angeletti D, Yewdell JW. Antibody Immunodominance: The Key to Understanding Influenza Virus Antigenic Drift. Viral Immunol. 2018; 31: 142–149. [PubMed: 29356618]

Bachmann MF, Odermatt B, Hengartner H, Zinkernagel RM. Induction of long-lived germinal centers associated with persisting antigen after viral infection. J Exp Med. 1996; 183: 2259–2269. [PubMed: 8642335]

Barnett BE, Staupe RP, Odorizzi PM, Palko O, Tomov VT, Mahan AE, Gunn B, Chen D, Paley MA, Alter G, et al. Cutting Edge: B Cell-Intrinsic T-bet Expression Is Required To Control Chronic Viral Infection. J Immunol. 2016; 197: 1017–1022. [PubMed: 27430722]

Chevrier S, Emslie D, Shi W, Kratina T, Wellard C, Karnowski A, Erikci E, Smyth GK, Chowdhury K, Tarlinton D, Corcoran LM. The BTB-ZF transcription factor Zbtb20 is driven by Irf4 to promote plasma cell differentiation and longevity. J Exp Med. 2014; 211: 827–840. [PubMed: 24711583]

Crotty S, Felgner P, Davies H, Glidewell J, Villarreal L, Ahmed R. Cutting edge: long-term B cell memory in humans after smallpox vaccination. J Immunol. 2003; 171: 4969–4973. [PubMed: 14607890]

Dugan HL, Stamper CT, Li L, Changrob S, Asby NW, Halfmann PJ, Zheng NY, Huang M, Shaw DG, Cobb MS, et al. Profiling B cell immunodominance after SARS-CoV-2 infection reveals antibody evolution to non-neutralizing viral targets. Immunity. 2021; 54: 1290–1303. e7 [PubMed: 34022127]

Frank GM, Angeletti D, Ince WL, Gibbs JS, Khurana S, Wheatley AK, Max EE, McDermott AB, Golding H, Stevens J, et al. A Simple Flow-Cytometric Method Measuring B Cell Surface Immunoglobulin Avidity Enables Characterization of Affinity Maturation to Influenza A Virus. MBio. 2015; 6 e01156 [PubMed: 26242629]

Fulcher DA, Basten A. B cell life span: a review. Immunol Cell Biol. 1997; 75: 446–455. [PubMed: 9429891]

Gaebler C, Wang Z, Lorenzi JCC, Muecksch F, Finkin S, Tokuyama M, Cho A, Jankovic M, Schaefer-Babajew D, Oliveira TY, et al. Evolution of antibody immunity to SARS-CoV-2. Nature. 2021; 591: 639–644. [PubMed: 33461210]

Europe PMC Funders Author Manuscripts

Gaya M, Barral P, Burbage M, Aggarwal S, Montaner B, Warren Navia A, Aid M, Tsui C, Maldonado P, Nair U, et al. Initiation of Antiviral B Cell Immunity Relies on Innate Signals from Spatially Positioned NKT Cells. Cell. 2018; 172: 517–533. e20 [PubMed: 29249358]

Gupta NT, Vander Heiden JA, Uduman M, Gadala-Maria D, Yaari G, Kleinstein SH. Change-O: a toolkit for analyzing large-scale B cell immunoglobulin repertoire sequencing data. Bioinformatics. 2015; 31: 3356–3358. [PubMed: 26069265]

Heesters BA, Chatterjee P, Kim YA, Gonzalez SF, Kuligowski MP, Kirchhausen T, Carroll MC. Endocytosis and recycling of immune complexes by follicular dendritic cells enhances B cell antigen binding and activation. Immunity. 2013; 38: 1164–1175. [PubMed: 23770227]

Heesters BA, Myers RC, Carroll MC. Follicular dendritic cells: dynamic antigen libraries. Nat Rev Immunol. 2014; 14: 495–504. [PubMed: 24948364]

Heesters BA, van der Poel CE, Das A, Carroll MC. Antigen Presentation to B Cells. Trends Immunol. 2016; 37: 844–854. [PubMed: 27793570]

Inoue T, Shinnakasu R, Kawai C, Ise W, Kawakami E, Sax N, Oki T, Kitamura T, Yamashita K, Fukuyama H, Kurosaki T. Exit from germinal center to become quiescent memory B cells depends on meta-bolic reprograming and provision of a survival signal. J Exp Med. 2021; 218 e20200866 [PubMed: 33045065]

Ise W, Fujii K, Shiroguchi K, Ito A, Kometani K, Takeda K, Kawakami E, Yamashita K, Suzuki K, Okada T, Kurosaki T. T Follicular Helper Cell-Germinal Center B Cell Interaction Strength Regulates Entry into Plasma Cell or Recycling Germinal Center Cell Fate. Immunity. 2018; 48: 702–715. e4 [PubMed: 29669250]

Jelley-Gibbs DM, Brown DM, Dibble JP, Haynes L, Eaton SM, Swain SL. Unexpected prolonged presentation of influenza antigens promotes CD4 T cell memory generation. J Exp Med. 2005; 202: 697–706. [PubMed: 16147980]

Jones DD, Wilmore JR, Allman D. Cellular Dynamics of Memory B Cell Populations: IgM^+ and IgG^+ Memory B Cells Persist Indefinitely as Quiescent Cells. J Immunol. 2015; 195: 4753–4759. [PubMed: 26438523]

Kim TS, Hufford MM, Sun J, Fu YX, Braciale TJ. Antigen persistence and the control of local T cell memory by migrant respiratory dendritic cells after acute virus infection. J Exp Med. 2010; 207: 1161–1172. [PubMed: 20513748]

Krishnamurty AT, Thouvenel CD, Portugal S, Keitany GJ, Kim KS, Holder A, Crompton PD, Rawlings DJ, Pepper M. Somatically Hypermutated Plasmodium-Specific $IgM(^+)$ Memory B Cells Are Rapid, Plastic, Early Responders upon Malaria Rechallenge. Immunity. 2016; 45: 402–414. [PubMed: 27473412]

Kuraoka M, Schmidt AG, Nojima T, Feng F, Watanabe A, Kitamura D, Harrison SC, Kepler TB, Kelsoe G. Complex Antigens Drive Permissive Clonal Selection in Germinal Centers. Immunity. 2016; 44: 542–552. [PubMed: 26948373]

Laidlaw BJ, Cyster JG. Transcriptional regulation of memory B cell differentiation. Nat Rev Immunol. 2021; 21: 209–220. [PubMed: 33024284]

Laidlaw BJ, Schmidt TH, Green JA, Allen CD, Okada T, Cyster JG. The Eph-related tyrosine kinase ligand Ephrin-B1 marks germinal center and memory precursor B cells. J Exp Med. 2017; 214: 639–649. [PubMed: 28143955]

Laidlaw BJ, Duan L, Xu Y, Vazquez SE, Cyster JG. The transcription factor Hhex cooperates with the corepressor Tle3 to promote memory B cell development. Nat Immunol. 2020; 21: 1082–1093. [PubMed: 32601467]

Lam KP, Kuhn R, Rajewsky K. In vivo ablation of surface immunoglobulin on mature B cells by inducible gene targeting results in rapid cell death. Cell. 1997; 90: 1073–1083. [PubMed: 9323135]

Leach S, Shinnakasu R, Adachi Y, Momota M, Makino-Okamura C, Ya-mamoto T, Ishii KJ, Fukuyama H, Takahashi Y, Kurosaki T. Requirement for memory B-cell activation in protection from heterologous influenza virus reinfection. Int Immunol. 2019; 31: 771–779. [PubMed: 31231764]

Levine AG, Mendoza A, Hemmers S, Moltedo B, Niec RE, Schizas M, Hoyos BE, Putintseva EV, Chaudhry A, Dikiy S, et al. Stability and function of regulatory T cells expressing the transcription factor T-bet. Nature. 2017; 546: 421–425. [PubMed: 28607488]

Luckey CJ, Bhattacharya D, Goldrath AW, Weissman IL, Benoist C, Mathis D. Memory T and memory B cells share a transcriptional program of self-renewal with long-term hematopoietic stem cells. Proc Natl Acad Sci USA. 2006; 103: 3304–3309. [PubMed: 16492737]

Mandel TE, Phipps RP, Abbot A, Tew JG. The follicular dendritic cell: long term antigen retention during immunity. Immunol Rev. 1980; 53: 29–59. [PubMed: 6162778]

Mathew NR, Jayanthan JK, Smirnov IV, Robinson JL, Axelsson H, Nakka SS, Emmanouilidi A, Czarnewski P, Yewdell WT, Schön K, et al. Single-cell BCR and transcriptome analysis after influenza infection reveals spatiotemporal dynamics of antigen-specific B cells. Cell Rep. 2021; 35 109286 [PubMed: 34161770]

Matsuda K, Huang J, Zhou T, Sheng Z, Kang BH, Ishida E, Griesman T, Stuccio S, Bolkhovitinov L, Wohlbold TJ, et al. Prolonged evolution of the memory B cell response induced by a replicating adenovirus-influenza H5 vaccine. Sci Immunol. 2019; 4 eaau2710 [PubMed: 31004012]

Mendoza A, Yewdell WT, Hoyos B, Schizas M, Bou-Puerto R, Michaels AJ, Brown CC, Chaudhuri J, Rudensky AY. Assembly of a spatial circuit of T-bet-expressing T and B lymphocytes is required for antiviral humoral immunity. Sci Immunol. 2021; 6 eabi4710 [PubMed: 34117110]

Mesin L, Ersching J, Victora GD. Germinal Center B Cell Dynamics. Immunity. 2016; 45: 471–482. [PubMed: 27653600]

Mesin L, Schiepers A, Ersching J, Barbulescu A, Cavazzoni CB, Angel-ini A, Okada T, Kurosaki T, Victora GD. Restricted Clonality and Limited Germinal Center Reentry Characterize Memory B Cell Reactivation by Boosting. Cell. 2020; 180: 92–106. e11 [PubMed: 31866068]

Müller-Winkler J, Mitter R, Rappe JCF, Vanes L, Schweighoffer E, Mo-hammadi H, Wack A, Tybulewicz VLJ. Critical requirement for BCR, BAFF, and BAFFR in memory B cell survival. J Exp Med. 2021; 218 e20191393 [PubMed: 33119032]

Oh JE, Iijima N, Song E, Lu P, Klein J, Jiang R, Kleinstein SH, Iwasaki A. Migrant memory B cells secrete luminal antibody in the vagina. Nature. 2019; 571: 122–126. [PubMed: 31189952]

Onodera T, Takahashi Y, Yokoi Y, Ato M, Kodama Y, Hachimura S, Kurosaki T, Kobayashi K. Memory B cells in the lung participate in protective humoral immune responses to pulmonary influenza virus reinfection. Proc Natl Acad Sci USA. 2012; 109: 2485–2490. [PubMed: 22308386]

Palese P. The genes of influenza virus. Cell. 1977; 10: 1–10. [PubMed: 837439]

Pape KA, Taylor JJ, Maul RW, Gearhart PJ, Jenkins MK. Different B cell populations mediate early and late memory during an endogenous immune response. Science. 2011; 331: 1203–1207. [PubMed: 21310965]

Peng SL, Szabo SJ, Glimcher LH. T-bet regulates IgG class switching and pathogenic autoantibody production. Proc Natl Acad Sci USA. 2002; 99: 5545–5550. [PubMed: 11960012]

Phan TG, Paus D, Chan TD, Turner ML, Nutt SL, Basten A, Brink R. High affinity germinal center B cells are actively selected into the plasma cell compartment. J Exp Med. 2006; 203: 2419–2424. [PubMed: 17030950]

Poon MML, Rybkina K, Kato Y, Kubota M, Matsumoto R, Bloom NI, Zhang Z, Hastie KM, Grifoni A, Weiskopf D, et al. SARS-CoV-2 infection generates tissue-localized immunological memory in humans. Sci Immunol. 2021; doi: 10.1126/sciimmunol.abl9105

Purtha WE, Tedder TF, Johnson S, Bhattacharya D, Diamond MS. Memory B cells, but not long-lived plasma cells, possess antigen specificities for viral escape mutants. J Exp Med. 2011; 208: 2599–2606. [PubMed: 22162833]

Riedel R, Addo R, Ferreira-Gomes M, Heinz GA, Heinrich F, Kummer J, Greiff V, Schulz D, Klaeden C, Cornelis R, et al. Discrete populations of isotype-switched memory B lymphocytes are maintained in murine spleen and bone marrow. Nat Commun. 2020; 11 2570 [PubMed: 32444631]

Roco JA, Mesin L, Binder SC, Nefzger C, Gonzalez-Figueroa P, Canete PF, Ellyard J, Shen Q, Robert PA, Cappello J, et al. Class-Switch Recombination Occurs Infrequently in Germinal Centers. Immunity. 2019; 51: 337–350. e7 [PubMed: 31375460]

Rothaeusler K, Baumgarth N. B-cell fate decisions following influenza virus infection. Eur J Immunol. 2010; 40: 366–377. [PubMed: 19946883]

Sakharkar M, Rappazzo CG, Wieland-Alter WF, Hsieh CL, Wrapp D, Esterman ES, Kaku CI, Wec AZ, Geoghegan JC, McLellan JS, et al. Prolonged evolution of the human B cell response to SARS-CoV-2 infection. Sci Immunol. 2021; 6 eabg6916 [PubMed: 33622975]

Schiemann B, Gommerman JL, Vora K, Cachero TG, Shulga-Morskaya S, Dobles M, Frew E, Scott ML. An essential role for BAFF in the normal development of B cells through a BCMA-independent pathway. Science. 2001; 293: 2111–2114. [PubMed: 11509691]

Schittek B, Rajewsky K. Maintenance of B-cell memory by long-lived cells generated from proliferating precursors. Nature. 1990; 346: 749–751. [PubMed: 2388695]

Schneider P, Takatsuka H, Wilson A, Mackay F, Tardivel A, Lens S, Cachero TG, Finke D, Beermann F, Tschopp J. Maturation of marginal zone and follicular B cells requires B cell activating factor of the tumor necrosis factor family and is independent of B cell maturation antigen. J Exp Med. 2001; 194: 1691–1697. [PubMed: 11733583]

Shinnakasu R, Inoue T, Kometani K, Moriyama S, Adachi Y, Nakayama M, Takahashi Y, Fukuyama H, Okada T, Kurosaki T. Regulated selection of germinal-center cells into the memory B cell compartment. Nat Immunol. 2016; 17: 861–869. [PubMed: 27158841]

Smith KG, Light A, Nossal GJ, Tarlinton DM. The extent of affinity maturation differs between the memory and antibody-forming cell compartments in the primary immune response. EMBO J. 1997; 16: 2996–3006. [PubMed: 9214617]

Sokal A, Chappert P, Barba-Spaeth G, Roeser A, Fourati S, Azzaoui I, Vandenberghe A, Fernandez I, Meola A, Bouvier-Alias M, et al. Maturation and persistence of the anti-SARS-CoV-2 memory B cell response. Cell. 2021; 184: 1201–1213. e14 [PubMed: 33571429]

Stone SL, Peel JN, Scharer CD, Risley CA, Chisolm DA, Schultz MD, Yu B, Ballesteros-Tato A, Wojciechowski W, Mousseau B, et al. T-bet Transcription Factor Promotes Antibody-Secreting Cell Differentiation by Limiting the Inflammatory Effects of IFN-γ on B Cells. Immunity. 2019; 50: 1172–1187. e7 [PubMed: 31076359]

Stuart T, Butler A, Hoffman P, Hafemeister C, Papalexi E, Mauck WM 3rd, Hao Y, Stoeckius M, Smibert P, Satija R. Comprehensive Integration of Single-Cell Data. Cell. 2019; 177: 1888–1902. e21 [PubMed: 31178118]

Suan D, Krautler NJ, Maag JLV, Butt D, Bourne K, Hermes JR, Avery DT, Young C, Statham A, Elliott M, et al. CCR6 Defines Memory B Cell Precursors in Mouse and Human Germinal Centers, Revealing Light-Zone Location and Predominant Low Antigen Affinity. Immunity. 2017; 47: 1142–1153. e4 [PubMed: 29262350]

Takatsuka S, Yamada H, Haniuda K, Saruwatari H, Ichihashi M, Renauld JC, Kitamura D. IL-9 receptor signaling in memory B cells regulates humoral recall responses. Nat Immunol. 2018; 19: 1025–1034. [PubMed: 30082831]

Taylor JJ, Pape KA, Jenkins MK. A germinal center-independent pathway generates unswitched memory B cells early in the primary response. J Exp Med. 2012; 209: 597–606. [PubMed: 22370719]

Taylor JJ, Pape KA, Steach HR, Jenkins MK. Humoral immunity. Apoptosis and antigen affinity limit effector cell differentiation of a single naïve B cell. Science. 2015; 347: 784–787. [PubMed: 25636798]

Tew JG, Mandel TE. Prolonged antigen half-life in the lymphoid follicles of specifically immunized mice. Immunology. 1979; 37: 69–76. [PubMed: 468304]

Tomayko MM, Steinel NC, Anderson SM, Shlomchik MJ. Cutting edge: hierarchy of maturity of murine memory B cell subsets. J Immunol. 2010; 185: 7146–7150. [PubMed: 21078902]

Turner DL, Cauley LS, Khanna KM, Lefrançois L. Persistent antigen presentation after acute vesicular stomatitis virus infection. J Virol. 2007; 81: 2039–2046. [PubMed: 17151119]

Turner JS, Zhou JQ, Han J, Schmitz AJ, Rizk AA, Alsoussi WB, Lei T, Amor M, McIntire KM, Meade P, et al. Human germinal centres engage memory and naive B cells after influenza vaccination. Nature. 2020; 586: 127–132. [PubMed: 32866963]

Turner JS, O'Halloran JA, Kalaidina E, Kim W, Schmitz AJ, Zhou JQ, Lei T, Thapa M, Chen RE, Case JB, et al. SARS-CoV-2 mRNA vaccines induce persistent human germinal centre responses. Nature. 2021; 596: 109–113. [PubMed: 34182569]

Viant C, Weymar GHJ, Escolano A, Chen S, Hartweger H, Cipolla M, Gazumyan A, Nussenzweig MC. Antibody Affinity Shapes the Choice between Memory and Germinal Center B Cell Fates. Cell. 2020; 183: 1298–1311. e11 [PubMed: 33125897]

Victora GD, Wilson PC. Germinal center selection and the antibody response to influenza. Cell. 2015; 163: 545–548. [PubMed: 26496601]

Wang Y, Bhattacharya D. Adjuvant-specific regulation of long-term antibody responses by ZBTB20. J Exp Med. 2014; 211: 841–856. [PubMed: 24711582]

Wang Y, Shi J, Yan J, Xiao Z, Hou X, Lu P, Hou S, Mao T, Liu W, Ma Y, et al. Germinal-center development of memory B cells driven by IL-9 from follicular helper T cells. Nat Immunol. 2017; 18: 921–930. [PubMed: 28650481]

Wang Z, Muecksch F, Schaefer-Babajew D, Finkin S, Viant C, Gaebler C, Hoffmann HH, Barnes CO, Cipolla M, Ramos V, et al. Naturally enhanced neutralizing breadth against SARS-CoV-2 one year after infection. Nature. 2021; 595: 426–431. [PubMed: 34126625]

Weisel FJ, Zuccarino-Catania GV, Chikina M, Shlomchik MJ. A Temporal Switch in the Germinal Center Determines Differential Output of Memory B and Plasma Cells. Immunity. 2016; 44: 116–130. [PubMed: 26795247]

Whittle JR, Wheatley AK, Wu L, Lingwood D, Kanekiyo M, Ma SS, Narpala SR, Yassine HM, Frank GM, Yewdell JW, et al. Flow cytometry reveals that H5N1 vaccination elicits cross-reactive stem-directed antibodies from multiple Ig heavy-chain lineages. J Virol. 2014; 88: 4047–4057. [PubMed: 24501410]

Wickham, H. ggplot2: Elegant Graphics for Data Analysis, Second Edition. Springer; 2009.

Wong R, Belk JA, Govero J, Uhrlaub JL, Reinartz D, Zhao H, Errico JM, D'Souza L, Ripperger TJ, Nikolich-Zugich J, et al. Affinity-Restricted Memory B Cells Dominate Recall Responses to Heterologous Fla-viviruses. Immunity. 2020; 53: 1078–1094. e7 [PubMed: 33010224]

Yewdell WT, Chaudhuri J. A transcriptional serenAID: the role of noncoding RNAs in class switch recombination. Int Immunol. 2017; 29: 183–196. [PubMed: 28535205]

Zammit DJ, Turner DL, Klonowski KD, Lefrancois L, Cauley LS. Residual antigen presentation after influenza virus infection affects CD8 T cell activation and migration. Immunity. 2006; 24: 439–449. [PubMed: 16618602]

Europe PMC Funders Author Manuscripts

Europe PMC Funders Author Manuscripts

Highlights

- Respiratory virus infection induces antiviral GCs that can persist for 5 months
- Persistent GCs continuously differentiate antiviral MBCs
- “Peak” and “late” GCs produce roughly equal numbers of long-lived antiviral MBCs
- Peak and late GCs produce ~1–5 long-lived antiviral MBCs per day

Europe PMC Funders Author Manuscripts

In brief

Yewdell et al. examine persistent germinal center responses induced by influenza A virus infection. Their findings reveal critical aspects of antiviral memory B cell differentiation that have direct implications for the development of optimal vaccination strategies that maximize antibody affinity maturation.

Europe PMC Funders Author Manuscripts

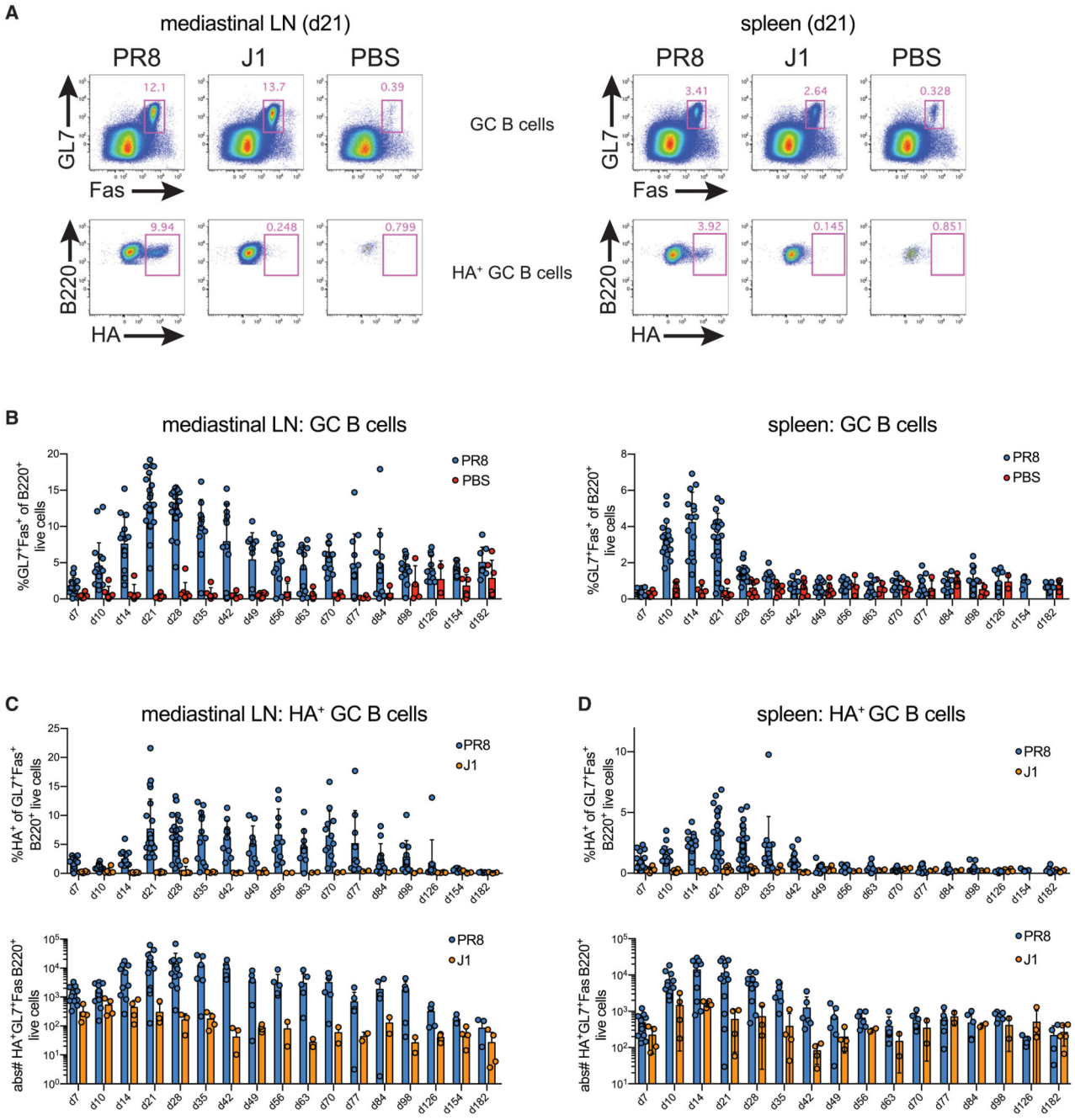

Figure 1. Temporal dynamics of the germinal center B cell response to influenza A virus infection

Mice were infected intranasally with 50 $TCID_{50}$ PR8 (blue), 50 $TCID_{50}$ J1 (orange), or PBS (red), and the mediastinal lymph node (mLN) and spleen were analyzed at the indicated time points post-infection.

(A) Representative gates for germinal center (GC) B cells ($GL7^+Fas^+$ of $B220^+$ live cells) (top), and hemagglutinin-specific (HA^+) GC B cells (HA^+ of $GL7^+Fas^+B220^+$ live cells) (bottom), in the mLN (left) and spleen (right).

(B) Quantification of GC B cell frequency within the mLN (left) and spleen (right).

(C and D) Quantification of HA^+ frequency within GC B cells (top), and their absolute number (bottom), within the mLN (C) and spleen (D).

The data for each time point in (A)–(D) are from, or representative of, 1–4 independent experiments, with 4–6 PR8-infected mice, 0–5 J1-infected mice, and 0–6 PBS controls per experiment, with each group containing approximately equal numbers of male and female mice. Error bars represent means ± SDs.

Europe PMC Funders Author Manuscripts

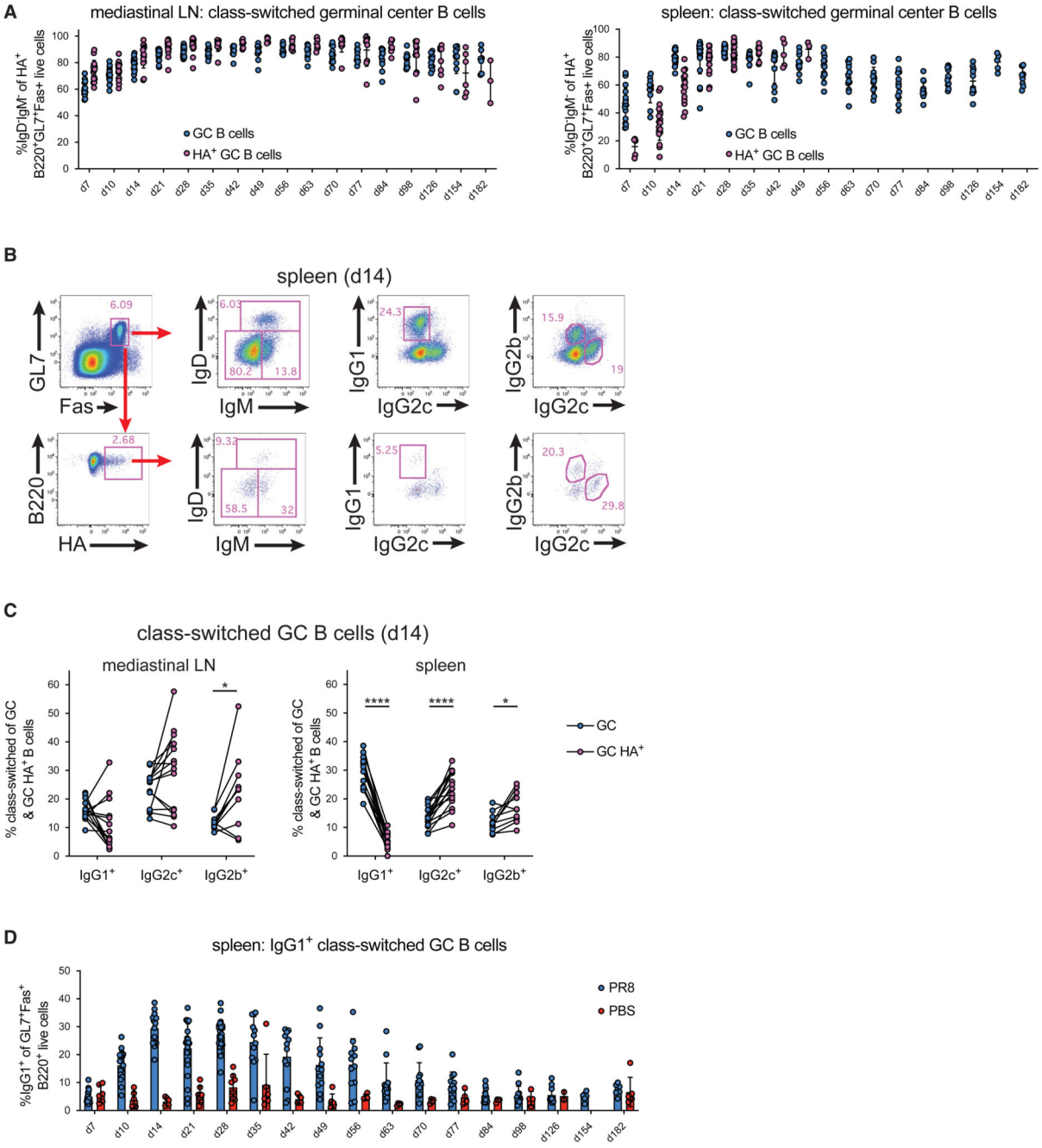

Figure 2. Differential class switching dynamics in the draining LN and spleen following influenza A virus infection

Mice were infected intranasally with 50 $TCID_{50}$ PR8 (blue and purple) or PBS (red), and the mLN and spleen were analyzed at the indicated time points post-infection.

(A) Quantification of class-switched B cells within bulk GC B cells (blue) or HA^+ GC B cells (orange) in the mLN (left) or spleen (right) following PR8 infection. The gating strategy is shown in Figure S1A.

Europe PMC Funders Author Manuscripts

(B and C) Representative gates for various class-switched isotypes among GC B cells ($GL7^+Fas^+$ of $B220^+$ live cells) and HA^+ GC B cells at d14 post-infection (B), quantified in (C).

(D) Quantification of $IgG1^+$ class-switched B cells among splenic GC B cells.

The data for each time point in (A)–(D) are from, or representative of, 1–4 independent experiments, with 4–6 PR8-infected mice per experiment and 0–6 PBS controls per experiment, with each group containing approximately equal numbers of male and female mice. Error bars represent means ± SDs. *$p < 0.05$, ****$p < 0.0001$; p values calculated using a paired t test.

Europe PMC Funders Author Manuscripts

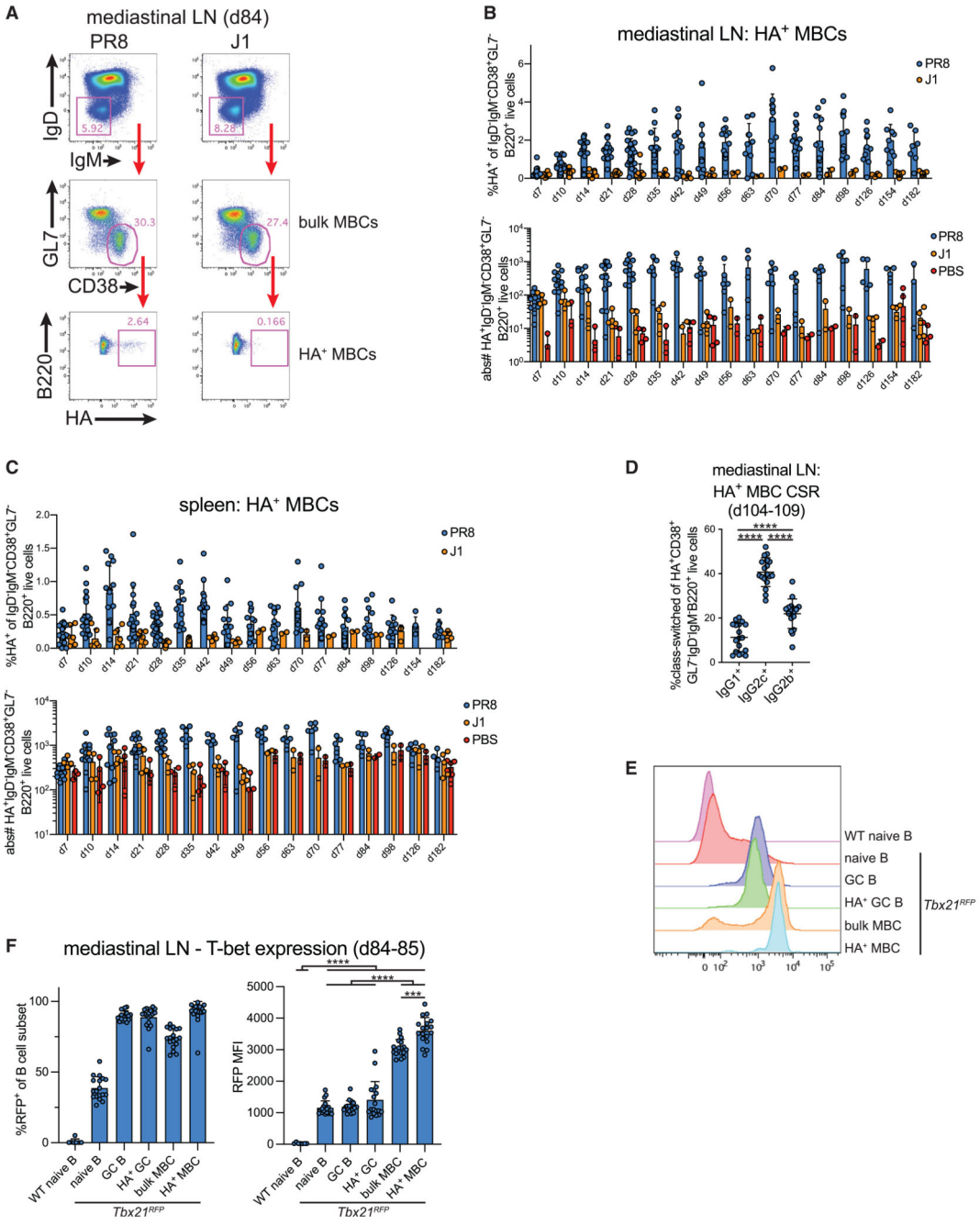

Figure 3. Temporal dynamics of memory B cell differentiation following influenza A virus infection

Mice were infected intranasally with 50 $TCID_{50}$ PR8 (blue), 50 $TCID_{50}$ J1 (orange), or PBS (red), and the mLN and spleen were analyzed at the indicated time points post-infection.

(A) Representative gates for HA^+ memory B cells (MBCs), gated on $B220^+$ live cells.

(B and C) Quantification of HA^+ MBC frequency (top), and their absolute number (bottom) within the mLN (B) and spleen (C).

(D) Quantification of class-switched B cell frequency among HA^+ MBCs.

Europe PMC Funders Author Manuscripts

(E and F) T-bet reporter mice (*Tbx21*^{RFP}) or wild-type (WT) controls were infected intranasally with 50 $TCID_{50}$ PR8, and the mLN was analyzed on d84-85 post-infection.
(E) Representative histograms depicting red fluorescent protein (RFP) expression among the indicated B cell subsets (parent gates shown in Figure S2C).
(F) Quantification of RFP^+ frequency among indicated B cell subsets (left), and RFP mean fluorescence intensity (MFI) among indicated T-bet^+ B cell subsets or WT naive B cells (right).
The data for each time point in (A)–(C) are from, or representative of, 1–4 independent experiments, with 4–6 PR8 infected mice, 0–5 J1 infected mice, and 0–6 PBS controls per experiment. The data for each time point in (D) are from 4 independent experiments, with 4–5 PR8-infected mice per experiment. The data for each time point in (E) and (F) are from 2 independent experiments, with 7–11 *Tbx21*^{RFP} PR8-infected mice, 3-4 WT PR8-infected mice, 4 *Tbx21*^{RFP} J1-infected mice, and 4 *Tbx21*^{RFP} PBS-infected mice per experiment. The data in (A)–(C), (E), and (F) contain approximately equal numbers of male and female mice; the data in (D) contain female mice only. Error bars represent means ± SDs. ***$p < 0.001$, ****$p < 0.0001$; p values calculated using a 1-way ANOVA with Tukey's multiple-comparisons test without pairing.

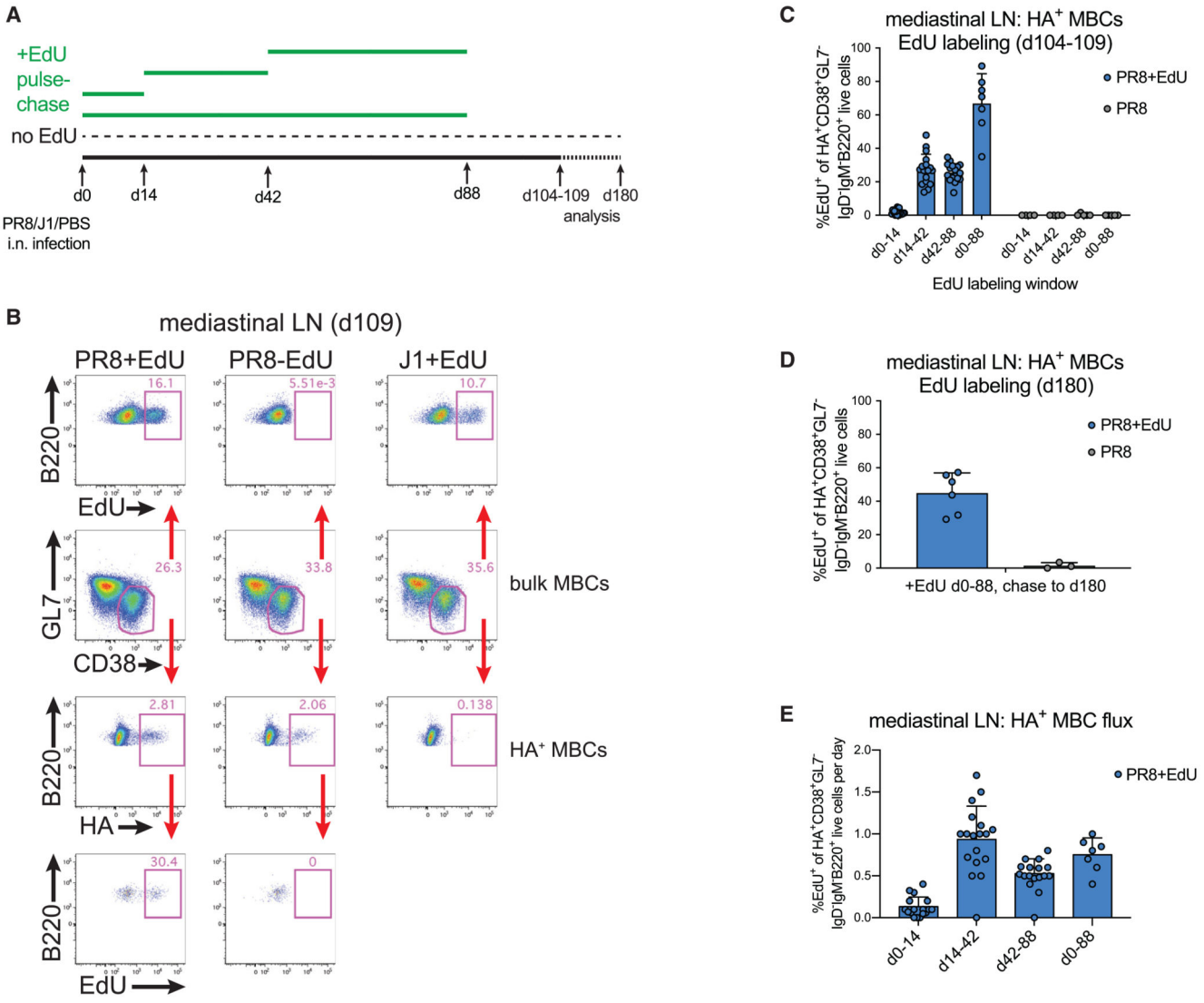

Figure 4. HA$^+$ MBCs continually differentiate from persistent GCs following influenza A virus infection

Following intranasal infection with 50 $TCID_{50}$ PR8, 50 $TCID_{50}$ J1, or PBS, EdU was added to drinking water during the indicated labeling windows, subsequently chased with normal water, and the mLN was analyzed at d104–109 or d180 post-infection.

(A) Pulse-chase experimental design. EdU labeling windows indicated in green.

(B) Representative gates for EdU$^+$ bulk MBCs and HA$^+$ MBCs, gated on IgD$^-$IgM$^-$B220$^+$ live cells.

(C and D) Quantification of EdU$^+$ frequency within HA$^+$ MBCs following EdU labeling during the indicated pulse windows at d104–109 (C) and d180 (D) post-infection.

(E) Normalization of the data shown in (C), wherein the frequency of EdU$^+$ cells among HA$^+$ MBCs is divided by the duration of the labeling window.

Data in (A)–(E) are from, or representative of, 1–2 independent experiments with 8–11 PR8-infected female mice per experiment. Error bars represent means ± SDs.

Europe PMC Funders Author Manuscripts

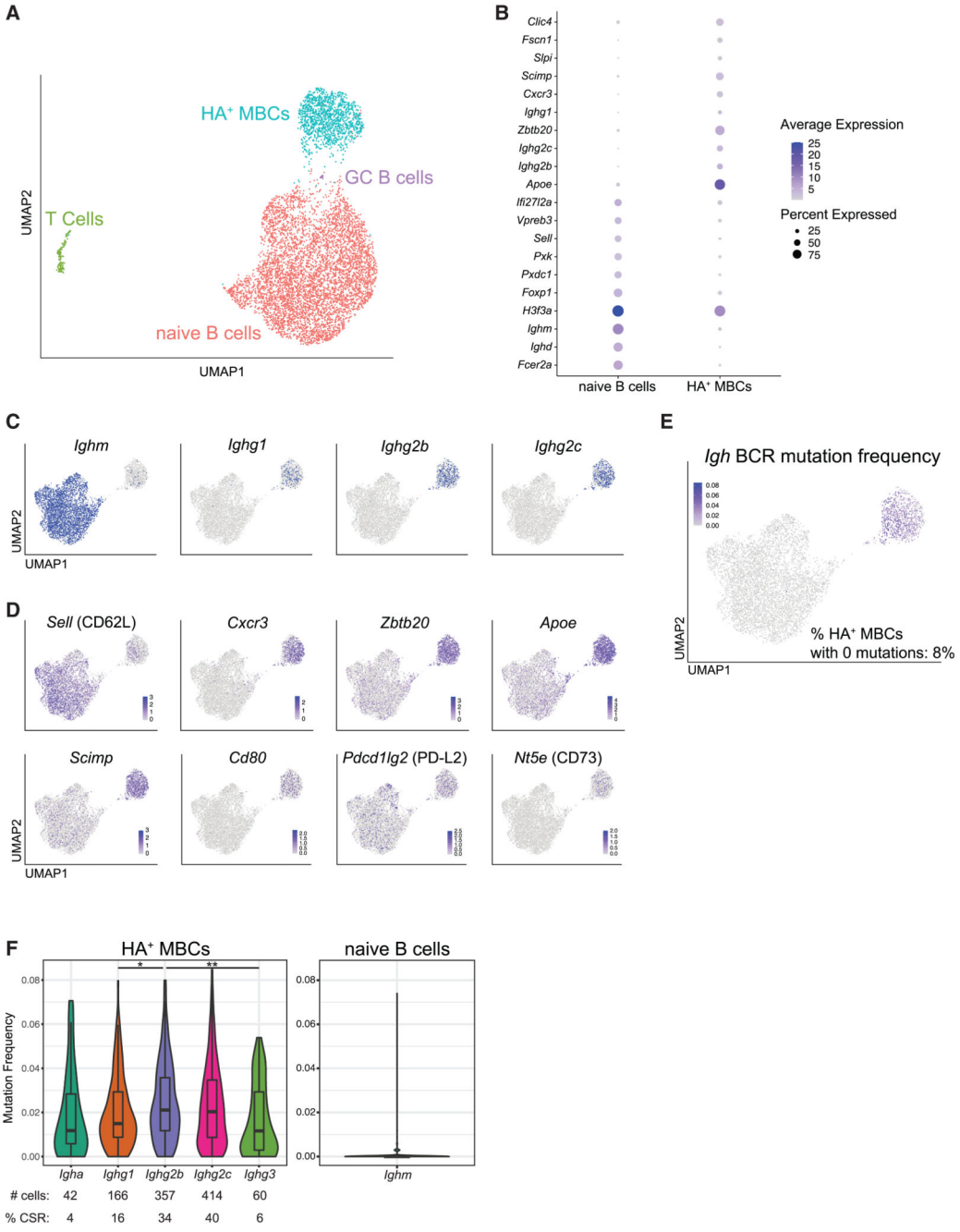

Figure 5. Single-cell B cell receptor and transcriptome analyses of long-lived HA$^+$ MBCs

Mice were infected intranasally with 50 $TCID_{50}$ PR8, and HA$^+$ MBCs and naive B cells were sorted from the mLN at d109 post-infection (gates shown in Figure S4A) and subjected to single-cell B cell receptor (BCR) and transcriptome analyses (see Method details).

(A) Uniform manifold approximation and projection (UMAP) of 5,421 sorted naive B cells and 1,326 HA$^+$ MBCs (T cell and GC B cell clusters removed for UMAPs in C–E).

(B) Expression of top 10 genes defining the naive B cell and HA$^+$ MBC clusters.

(C) BCR isotype expression displayed on a UMAP, derived from BCR-sequencing data.

(D) Expression of selected genes displayed on a UMAP.
(E and F) Analysis of Igh BCR mutation frequency (mutations per base pair), displayed on a UMAP (E) or violin plots parsed by BCR isotype (F). The number of cells detected expressing each isotype, and their frequency among HA^+ MBCs, shown below (F).
Data in (A)–(F) are pooled from 2 independent experiments, with 30–32 PR8-infected female mice per experiment. *$p < 0.05$, **$p < 0.01$; p values calculated using a 1-way ANOVA with Tukey's multiple-comparisons test without pairing.

Europe PMC Funders Author Manuscripts